J. Fluid Mech. (2013), *vol.* 737, *pp.* 249–279.
doi:10.1017/jfm.2013.572

Linear stability analysis of channel flow of viscoelastic Oldroyd-B and FENE-P fluids

Mengqi Zhang[1],‡, **Iman Lashgari**[1], **Tamer A. Zaki**[2] **and Luca Brandt**[1],†

[1]Linné Flow Centre and SeRC (Swedish e-Science Research Centre),
KTH Mechanics, S-100 44 Stockholm, Sweden
[2]Mechanical Engineering, Imperial College, London SW7 2AZ, UK

(Received 1 February 2013; revised 15 September 2013; accepted 25 October 2013)

We study the modal and non-modal linear instability of inertia-dominated channel flow of viscoelastic fluids modelled by the Oldroyd-B and FENE-P closures. The effects of polymer viscosity and relaxation time are considered for both fluids, with the additional parameter of the maximum possible extension for the FENE-P. We find that the parameter explaining the effect of the polymer on the instability is the ratio between the polymer relaxation time and the characteristic instability time scale (the frequency of a modal wave and the time over which the disturbance grows in the non-modal case). Destabilization of both modal and non-modal instability is observed when the polymer relaxation time is shorter than the instability time scale, whereas the flow is more stable in the opposite case. Analysis of the kinetic energy budget reveals that in both regimes the production of perturbation kinetic energy due to the work of the Reynolds stress against the mean shear is responsible for the observed effects where polymers act to alter the correlation between the streamwise and wall-normal velocity fluctuations. In the subcritical regime, the non-modal amplification of streamwise elongated structures is still the most dangerous disturbance-growth mechanism in the flow and this is slightly enhanced by the presence of polymers. However, viscoelastic effects are found to have a stabilizing effect on the amplification of oblique modes.

Key words: instability, non-Newtonian flows

1. Introduction

The effect of elasticity on the instability and transition of both inertialess and inertial flows of viscoelastic fluids is not well understood. Except for the few studies mentioned below, most of the previous stability analysis considered inertialess flow configurations. In the inertial regime, the focus has been on the turbulent flow of a viscoelastic solution to understand turbulent drag reduction: see the early discovery by Toms (1949) and the review by White & Mungal (2008). Here, we focus on inertial flows, and in particular the linear instability behaviour of polymeric inertial

† Email address for correspondence: luca@mech.kth.se

‡ Current address: Département Fluides, Thermique, Combustion, Institut PPrime, CNRS–Université de Poitiers–ENSMA, Poitiers, France.

channel flow. We investigate how the modal and non-modal amplification of initial perturbations of different spatial scales are affected by the polymer additives.

1.1. *Hydrodynamic stability of elastic-dominated inertialess flows*

Over the past decades, there has been a growing interest in the study of instabilities in viscoelastic fluids due to their significant fundamental and practical implications. While transition in Newtonian fluids is governed by the fluid inertia, non-Newtonian inertialess flows might experience instabilities due to the action of elasticity, so-called elastic instabilities: see the review by Shaqfeh (1996) and the introduction in Larson (2000). These instabilities can lead to elastic turbulence, a flow regime characterized by broad range of spatial and temporal scales even at vanishing *Re* (Groisman & Steinberg 2001). From a practical point of view, the knowledge and control of elastic instabilities can be used to increase the efficiency of several industrial processes such as extrusion, coating and film blowing as well as mixing in microfluidic devices (Larson 1992).

Elastic instabilities have been observed in several configurations displaying curvature of the flow streamlines. In curvilinear flows, the stretched polymer molecules exert an extra pressure toward the centre of the curvature. Laminar flow becomes linearly unstable when these extra forces overcome viscous friction (Morozov & Saarloos 2005). Larson, Shaqfeh & Muller (1990) studied the viscoelastic instability of the Oldroyd-B inertialess Taylor–Couette flow. For high Deborah numbers (the Deborah number is the ratio between the polymer relaxation time and the flow time scale), the interaction between the velocity fluctuations and the first normal stress difference results in the appearance of toroidal waves. Groisman & Steinberg (2004) conducted an experiment on elastic-dominated flows with weakly curved streamlines, i.e. swirling flow, Taylor–Couette flow and Dean flow. The appearance of random fluctuations was shown to characterize the elastic turbulence. Arratia *et al.* (2006) documented the viscoelastic effects on the stability of the flow in a microchannel junction. These authors found elastic instabilities in the form of symmetry breaking and large velocity fluctuations. The appearance of elastic turbulence is related to large elastic stresses by Burghelea, Segre & Steinberg (2006), who considered the flow between two disks. Interestingly, Berti *et al.* (2008) studied numerically the Kolmogorov flow of Oldroyd-B fluids and observed two-dimensional elastic instabilities at low inertia and for sufficiently high Weissenberg numbers (the Weissenberg number defined as the product of the polymer relaxation time and the shear rate) also in a flow without curved streamlines.

Elastic instabilities have also been studied in parallel wall-bounded shear flow: Sureshkumar *et al.* (1999) investigated both the linear and nonlinear stability of creeping viscoelastic Couette flow. The non-normal viscoelastic dynamics lead to the transient amplification of the perturbation energy and finite amplitude instability as observed for inertial Newtonian flows. The Poiseuille flow of upper convected Maxwell (UCM) fluids exhibits a nonlinear instability due to the action of normal viscoelastic stresses (see Meulenbroek *et al.* 2004). Employing a weakly nonlinear analysis, these authors found the threshold amplitude of the velocity fluctuations beyond which the instability arises. Transient growth analysis of inertialess Couette and Poiseuille flow of viscoelastic Oldroyd-B fluids was studied by Jovanović & Kumar (2010). The contribution of both velocity and polymer stress fluctuations, especially the streamwise components, are responsible for the large amplification of the energy. The wall-normal fluctuation of the polymer stress generates the largest transient growth, and the streamwise component is the most sensitive to the

elasticity. More recently, Jovanović & Kumar (2011) performed a stochastic analysis of disturbances in an elastic-dominated channel flow. Employing the Oldroyd-B constitutive model, they found a large velocity fluctuation variance also in the case of weak inertia. The stretching of the polymer molecules results in a lift-up of the disturbances similar to that in inertia-dominated Newtonian flows.

1.2. *Hydrodynamic stability of viscoelastic-inertial flows*

Although the hydrodynamics of viscoelastic fluids are strongly affected by the balance between inertia and elastic forces in the flow, the effect of elasticity on the stability of inertial flows has not been completely established, especially the non-modal flow behaviour. Among early investigations, we note the work by Porteous & Denn (1972) and Ho & Denn (1977) on the viscoelastic Poiseuille flow and by Renardy & Renardy (1986) on Couette flow. In those studies the main focus was on the choice of the constitutive model and modal stability to infinitesimal disturbances.

Inertial effects destabilize the purely elastic Dean and Taylor–Couette flows (Joo & Shaqfeh 1992). The opposite behaviour is reported in the work by Sureshkumar & Beris (1995), who show the large destabilizing effects of elasticity in Poiseuille flow of upper convected Maxwell fluids. Blonce (1997) employed a linear analysis to study the viscoelastic effects on the stability of Poiseuille flow of Giesekus fluids. A destabilization is induced by the elasticity in the inertial regime, i.e. $Re = O(10^3)$. A more complete analysis of the effect of elasticity on the critical Reynolds number of Poiseuille flow is reported by Sadanandan & Sureshkumar (2002). The viscoelastic shear and normal stress perturbations exhibit opposite behaviours at the Reynolds-elasticity neutral conditions. For higher Deborah numbers, the dissipative effect of the viscoelastic shear stress becomes dominant and the critical Reynolds number increases, as is further documented and explained in the current work by considering the budget of the perturbation kinetic energy. The time-evolution of two-dimensional disturbances of finite amplitude in viscoelastic Poiseuille and Couette flow is investigated by Atalik & Keunings (2002), using a nonlinear analysis. It is shown that the elasticity induces first destabilization and then stabilization of the periodic regime which is established beyond the critical point. The critical Reynolds number decreases when the ratio between the polymer viscosity and the total viscosity increases.

For the Newtonian, Couette and Poiseuille flows, it is well known that the linear stability analysis cannot predict the transition observed in the experiments. The non-normality of the linearized operator results in the transient amplification of the disturbances and promotes subcritical transition (see e.g. Trefethen *et al.* 1993; Schmid & Henningson 2001). Therefore, the analysis of the non-modal disturbance amplification in the viscoelastic channel flow is important to the understanding of the early stage of transition to turbulence and its modifications with respect to the Newtonian case. The energy density in a channel flow of Oldroyd-B fluid was studied by Hoda, Jovanović & Kumar (2008). It was observed that increasing the ratio between the viscosity of the solvent and the total viscosity decreases the energy amplification. The opposite behaviour was observed when increasing the Reynolds and elasticity numbers. A viscoelastic channel flow may become unstable in the weakly inertial regime due to the large amplification of elastic energy. More recently, these authors extended their work to the frequency response analysis of Oldroyd-B channel flow (Hoda, Jovanovic & Kumar 2009). This componentwise input–output analysis suggests that the exchange of energy between the polymer stress component, τ_{xy}, and the wall-normal gradient of the streamwise velocity, $\partial_y u$, contributes most to the energy amplification of streamwise elongated disturbances.

In most of the stability analysis of viscoelastic flows, the upper convected Maxwell (UCM) and the Oldroyd-B constitutive models have been employed. The choice of the constitutive model affects the results of the stability analysis. For example the Oldroyd-B model presents more stabilization than the UCM model in Poiseuille flow, when the solvent viscosity is taken into account (Sureshkumar & Beris 1995). In the present work we investigate the modal and non-modal stability of both FENE-P and Oldroyd-B fluids in channel flow. FENE-P includes an upper bound for the extension of polymer molecules and can more reliably represent dilute polymer solutions where significant drag reduction in the turbulent regime is observed (De Angelis, Casciola & Piva 2002; Dubief *et al.* 2004). A complete study is presented in order to illustrate the effects of the different rheological parameters on the flow stability. The results are verified and examined by means of an energy budget analysis. The only linear stability analyses of the FENE-P fluids have been performed in Arora & Khomami (2005) and very recently in Lieu, Jovanovic & Kumar (2013) on the inertialess regime of Couette flow. The focus of the present work is on the stability analysis of the FENE-P Poiseuille flow in the inertia-dominated regime, $Re > 2000$.

This paper is organized as follows. We present the problem formulation and the governing equations in § 2. The numerical model and its validation are reported in § 3. We show the results of modal and non-modal analysis in §§ 4 and 5 respectively, and provide a summary of the main conclusions in § 6.

2. Problem formulation

2.1. *Governing equations*

In our analysis, we use the Oldroyd-B and FENE-P models for viscoelastic fluids. The first model has been adopted by several authors for linear stability studies whereas only the studies of Arora & Khomami (2005) and Lieu *et al.* (2013) are devoted to the stability analysis of FENE-P fluids. The Oldroyd-B model does not impose a restriction on the extensibility of the polymer molecules and allows an unphysical infinite length. The finitely extensible nonlinear elastic (FENE) model imposes a finite extension of the polymer, but entails a statistical closure for the restoring force, for example the Peterlin closure (FENE-P). In these models, the polymer chain is represented as an elastic dumbbell with the two beads at each end connected with an entropic spring. The conformation tensor $\bar{C}^*_{ij} = \langle \bar{R}^*_i \bar{R}^*_j \rangle$, where $\bar{R}$ is the end-to-end vector of each molecule, describes the dynamics of the polymers. Here, the superscript star * represents dimensional quantities and the angular brackets denote the average over thermal noise. The conformation tensor is symmetric with six independent components in three dimensions and its trace, $\mathrm{tr}(\bar{\boldsymbol{C}})$, is a measure of the squared polymer elongation, which is proportional to the elastic energy stored in the molecule. The polymeric stress tensor is proportional to the deviation of the conformation tensor from its equilibrium state; in the Oldroyd-B model (Bird *et al.* 1987),

$$\bar{\boldsymbol{\tau}}^*_p = \frac{\mu_p H}{\lambda k_B T}(\bar{\boldsymbol{C}}^* - \bar{\boldsymbol{C}}^{*eq}). \tag{2.1}$$

In this definition, H is the spring constant of the elastic dumbbell, k_B is the Boltzmann constant and T is the temperature, λ is the relaxation time of the polymer molecules and μ_p is the additional fluid viscosity due to the polymer. Non-dimensionalizing $\bar{\boldsymbol{C}}^*$ by $k_B T/H$ and $\bar{\boldsymbol{\tau}}^*_p$ by $\mu_p U_c/L_c$ (U_c is the flow characteristic velocity and L_c is the flow

characteristic length), we obtain

$$\bar{\boldsymbol{\tau}}_p = \frac{\bar{\boldsymbol{C}} - \boldsymbol{I}}{W} \quad \text{(Oldroyd-B model)}. \tag{2.2}$$

Similarly, for the FENE-P model we obtain

$$\bar{\boldsymbol{\tau}}_p = \frac{f\bar{\boldsymbol{C}} - \boldsymbol{I}}{W} \quad \text{(FENE-P model)}, \tag{2.3}$$

where f is the Peterlin function and W is the Weissenberg number defined as the ratio between the polymer relaxation time and the flow convective time scale:

$$W \equiv \frac{\lambda U_c}{L_c}. \tag{2.4}$$

In the FENE-P model, the maximum extensibility of the polymer is denoted by L, and is typically much larger than the size of the polymer molecules in the coiled non-stretched state. The Peterlin function

$$f \equiv \frac{1}{1 - \dfrac{\bar{C}_{kk}}{L^2}} \tag{2.5}$$

confines the polymer extensibility to be less than the maximum extensibility L, and $\bar{C}_{kk} = \bar{C}_{11} + \bar{C}_{22} + \bar{C}_{33}$ is the trace of the base-state conformation tensor. Note that the dimensionless equilibrium state, $\bar{\boldsymbol{C}}^{*eq}$, is the coiled state corresponding to the identity matrix.

The non-dimensional constitutive equations for the evolution of the conformation tensor in the Oldroyd-B and FENE-P models read

$$\frac{\partial \bar{\boldsymbol{C}}}{\partial t} + \bar{\boldsymbol{u}} \cdot \nabla \bar{\boldsymbol{C}} - \bar{\boldsymbol{C}} \cdot (\nabla \bar{\boldsymbol{u}}) - (\nabla \bar{\boldsymbol{u}})^{\mathrm{T}} \cdot \bar{\boldsymbol{C}} = -\bar{\boldsymbol{\tau}}_p, \tag{2.6}$$

where $\bar{\boldsymbol{\tau}}_p$ is related to the conformation tensor by (2.2) and (2.3). The left-hand side of this evolution equation is the upper convective time derivative acting on the conformation tensor. Therefore, (2.6) expresses the balance between the transport and stretching of the polymer molecules by the flow $\bar{\boldsymbol{u}}$ and the relaxation with characteristic time λ.

The polymeric stress introduced above reacts back on the flow. The continuity and Navier–Stokes equations for an incompressible fluid read

$$\nabla \cdot \bar{\boldsymbol{u}} = 0, \tag{2.7}$$

$$\frac{\partial \bar{\boldsymbol{u}}}{\partial t} + \bar{\boldsymbol{u}} \cdot \nabla \bar{\boldsymbol{u}} = -\nabla \bar{p} + \frac{\beta}{Re} \nabla^2 \bar{\boldsymbol{u}} + \frac{1-\beta}{Re} \nabla \cdot \bar{\boldsymbol{\tau}}_p. \tag{2.8}$$

In the equations above we use the channel centreline velocity as the characteristic flow speed U_c, the channel half-width as the length scale L_c, the time scale $t = L_c/U_c$ and the reference pressure ρU_c^2. The parameter β is the viscosity ratio, defined as the ratio between the solvent viscosity μ_s and the total viscosity $\mu = \mu_s + \mu_p$. The Reynolds number is defined as $Re = \rho U_c L_c/\mu$.

In order to perform the linear stability analysis, we decompose the flow velocities, pressure and the components of the polymer conformation tensor and stress into base state and infinitesimal perturbations, $\bar{\boldsymbol{u}} = \boldsymbol{U} + \boldsymbol{u}$, $\bar{p} = P + p$, $\bar{\boldsymbol{C}} = \boldsymbol{C} + \boldsymbol{c}$, $\bar{\boldsymbol{\tau}} = \boldsymbol{T} + \boldsymbol{\tau}$, where capital letters indicate the base state and small letters denote the fluctuating components.

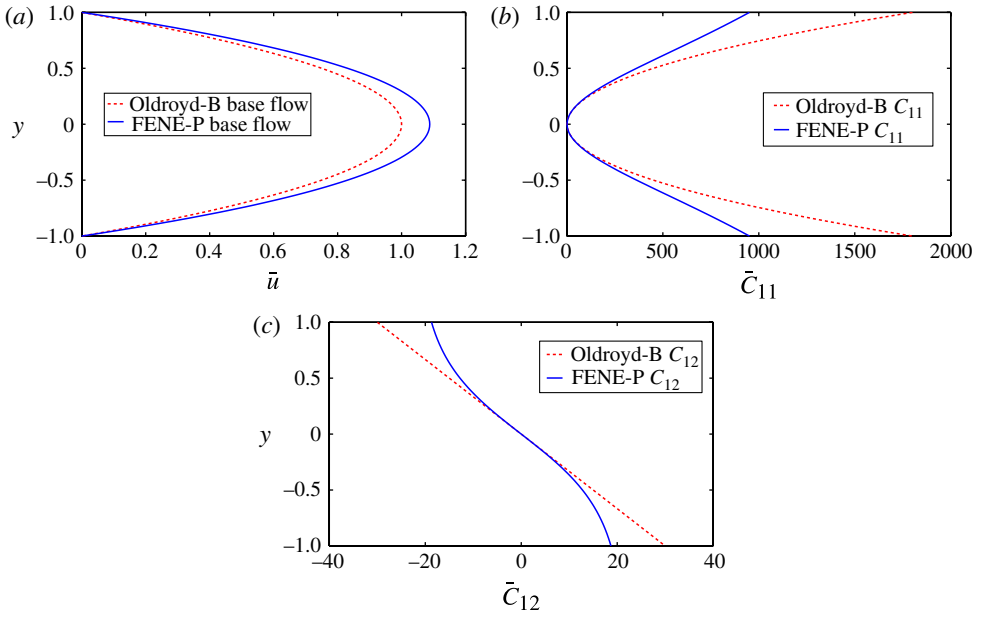

FIGURE 1. (Colour online) Base flow configuration for channel flow of the Oldroyd-B (dashed red line) and FENE-P (solid blue line) fluids at $W = 15$, $\beta = 0.5$, $L = 60$, $Re = 5000$. (*a*) Streamwise velocity. (*b*) $\bar{C}_{11}$ and (*c*) $\bar{C}_{12}$ components of the conformation tensor.

2.2. *Base flow*

We study plane channel flow where x, y, z represent the streamwise, wall-normal and spanwise directions, and $\bar{\boldsymbol{u}} = (\bar{u}, \bar{v}, \bar{w})$ are the corresponding velocity components.

For the Oldroyd-B model, the base flow velocity coincides with the Poiseuille parabolic solution $U = 1 - y^2$. An explicit expression can be derived for the conformation tensor from the equations above in the case of a steady parallel base flow $U = U(y)$

$$\boldsymbol{C} = \begin{pmatrix} 2W^2U'^2 + 1 & WU' & 0 \\ WU' & 1 & 0 \\ 0 & 0 & 1 \end{pmatrix}, \tag{2.9}$$

where U' is the wall-normal derivative of the base flow velocity. The stress tensor is readily obtained from (2.2).

2.2.1. *Channel flow of FENE-P fluids*

Unlike Oldroyd-B, the base flow velocity and the conformation tensor are both modified in the FENE-P model (see figure 1). The polymer molecules experience a larger stretching in the Oldroyd-B fluids than in FENE-P counterpart for the same rheological parameters.

An analytical solution for channel flow is presented in Cruz, Pinho & Oliveira (2005) and summarized below. For a two-dimensional flow (the subscript p in the elastic stress tensor will be omitted in the following),

$$T_{23} = T_{13} = T_{22} = T_{33} = 0, \tag{2.10}$$

and

$$T_{11} = 2C_{12}U', \quad T_{12} = 2C_{22}U'. \tag{2.11}$$

From the definition of the polymer stress, $C_{12}/C_{22} = WT_{12}$ and $T_{11} = 2WT_{12}^2$. Writing C_{22} in terms of T_{12}, and combining (2.11) with the x-component of the Navier–Stokes equations (2.8), we obtain

$$T_{12}^3 + \frac{L^2}{2W^2}\left(1 + \frac{3}{L^2} + \frac{1-\beta}{\beta}\right)T_{12} - \frac{L^2}{2}\frac{\mathrm{d}p}{\mathrm{d}x}\frac{Re}{\beta}\frac{1}{W^2}y = 0. \tag{2.12}$$

Once T_{12} (and hence T_{11}) is evaluated, the other components of the conformation tensor can be calculated as

$$C_{ij} = (WT_{ij} + \delta_{ij})\left(1 - \frac{C_{kk}}{L^2}\right). \tag{2.13}$$

The streamwise velocity is obtained by substituting T_{12} into the momentum equation (2.8) and integrating along the y-direction,

$$U(y) = -\frac{Re}{2\beta}\frac{\mathrm{d}p}{\mathrm{d}x}(1-y^2) - \frac{1-\beta}{\beta}\frac{3}{8C}(F_+G_-|_{-1}^{y} + F_-G_+|_{-1}^{y}), \tag{2.14}$$

where

$$F_+ = (Cy + \sqrt{C^2y^2 + A^3})^{1/3}, \quad F_- = (Cy - \sqrt{C^2y^2 + A^3})^{1/3}, \tag{2.15}$$

$$G_+ = 3Cy + \sqrt{C^2y^2 + A^3}, \quad G_- = 3Cy - \sqrt{C^2y^2 + A^3}, \tag{2.16}$$

and

$$A = \frac{L^2}{6W^2}\left(\frac{3}{L^2} + \frac{1}{\beta}\right), \quad C = \frac{L^2}{4}\frac{\mathrm{d}p}{\mathrm{d}x}\frac{Re}{\beta}\frac{1}{W^2}. \tag{2.17}$$

2.3. *Linear stability problem*

Since the flow is homogeneous in the streamwise and spanwise directions, we assume wave-like perturbations of the form

$$\phi(x, y, z, t) = \tilde{\phi}(y, t)\mathrm{e}^{\mathrm{i}\alpha x + \mathrm{i}\gamma z}. \tag{2.18}$$

The symbol tilde $\tilde{}$ represents the complex wall-normal shape function, α is the real-valued streamwise wavenumber, γ is the real-valued spanwise wavenumber, and ω is the complex circular frequency of the perturbation.

Linearization is applied both to the Navier–Stokes equations (2.8) and to the evolution equation for the polymer conformation tensor (2.6). Using the decomposition above, the linearized equations for the flow of an Oldroyd-B fluid is

$$\frac{\partial \boldsymbol{u}}{\partial t} + \boldsymbol{U}\cdot\nabla\boldsymbol{u} + \boldsymbol{u}\cdot\nabla\boldsymbol{U} = -\nabla p + \frac{\beta}{Re}\nabla^2\boldsymbol{u} + \frac{1-\beta}{Re\,W}\nabla\cdot\boldsymbol{c}, \tag{2.19}$$

whereas adopting the FENE-P closure yields

$$\frac{\partial \boldsymbol{u}}{\partial t} + \boldsymbol{U}\cdot\nabla\boldsymbol{u} + \boldsymbol{u}\cdot\nabla\boldsymbol{U} = -\nabla p + \frac{\beta}{Re}\nabla^2\boldsymbol{u} + \frac{1-\beta}{Re\,W}\nabla\cdot(f\boldsymbol{c} + f'\boldsymbol{C}). \tag{2.20}$$

In the linearized equation, the quadratic terms are neglected and f' is defined by the first term in the Taylor series of the Peterlin function, $f = f(C_{kk})$:

$$f' = \left.\frac{\partial f}{\partial C_{11}}\right|_B c_{11} + \left.\frac{\partial f}{\partial C_{22}}\right|_B c_{22} + \left.\frac{\partial f}{\partial C_{33}}\right|_B c_{33}, \tag{2.21}$$

where the subscript B refers to the base flow quantities. By eliminating the pressure term from the momentum equation (2.19), we can obtain the classical Orr–Sommerfeld (O–S) and Squire (Sq) system for the wall-normal velocity and vorticity $\eta \equiv \partial u/\partial z - \partial w/\partial x$ modified for polymeric Oldroyd-B fluids (and similarly for the FENE-P model):

$$\begin{aligned}\frac{\partial}{\partial t}\nabla^2 v = &\left[-U\frac{\partial}{\partial x}\nabla^2 + U''\frac{\partial}{\partial x} + \frac{\beta}{Re}\nabla^4\right] v \\ &+ \frac{1-\beta}{ReW}\left[\frac{\partial}{\partial x_j}\nabla^2 c_{jy} - \frac{\partial^3 c_{jx}}{\partial x_j \partial x \partial y} - \frac{\partial^2 c_{jy}}{\partial x_j \partial y^2} - \frac{\partial^2 c_{jz}}{\partial x_j \partial x \partial z}\right],\end{aligned} \tag{2.22}$$

$$\frac{\partial}{\partial t}\eta = -U\frac{\partial}{\partial x}\eta - U'\frac{\partial v}{\partial z} + \frac{\beta}{Re}\nabla^2\eta + \frac{1-\beta}{ReW}\left(\frac{\partial^2 c_{xj}}{\partial x_j \partial z} - \frac{\partial^2 c_{zj}}{\partial x_j \partial x}\right). \tag{2.23}$$

Here Einstein summation is implied when using the repeated index j. The boundary conditions for the wall-normal velocity and normal vorticity are $v = \partial/\partial y v = \eta = 0$. No boundary condition is necessary for the conformation tensor or the polymer stress tensor since (2.24) and (2.25) are of hyperbolic nature and there is no y-derivative for c.

The linearized constitutive equations for the conformation tensor are derived in the same way:

$$\frac{\partial \boldsymbol{c}}{\partial t} + \boldsymbol{u}\cdot\nabla\boldsymbol{C} + \boldsymbol{U}\cdot\nabla\boldsymbol{c} - \boldsymbol{c}\cdot\nabla\boldsymbol{U} - \boldsymbol{C}\cdot\nabla\boldsymbol{u} - (\nabla\boldsymbol{U})^{\mathrm{T}}\cdot\boldsymbol{c} - (\nabla\boldsymbol{u})^{\mathrm{T}}\cdot\boldsymbol{C} = -\frac{\boldsymbol{c}}{W}, \tag{2.24}$$

and

$$\begin{aligned}&\frac{\partial \boldsymbol{c}}{\partial t} + \boldsymbol{u}\cdot\nabla\boldsymbol{C} + \boldsymbol{U}\cdot\nabla\boldsymbol{c} - \boldsymbol{c}\cdot\nabla\boldsymbol{U} - \boldsymbol{C}\cdot\nabla\boldsymbol{u} \\ &\quad - (\nabla\boldsymbol{U})^{\mathrm{T}}\cdot\boldsymbol{c} - (\nabla\boldsymbol{u})^{\mathrm{T}}\cdot\boldsymbol{C} = -\frac{f'\boldsymbol{C} + f\boldsymbol{c}}{W},\end{aligned} \tag{2.25}$$

for Oldroyd-B and FENE-P respectively, with the same left-hand side. The FENE-P model reduces to the Oldroyd-B model at large L, and indeed (2.25) reduces to (2.24) as $L \to \infty$, $f = 1$ and $f' = 0$.

For clarity, we let $\tilde{\phi} = (\tilde{v}, \tilde{\eta}, \tilde{c}_{11}, \tilde{c}_{22}, \tilde{c}_{33}, \tilde{c}_{12}, \tilde{c}_{13}, \tilde{c}_{23})^{\mathrm{T}}$ denote the eight-component vector containing the unknown fluid velocities and polymer state, and rewrite the linearized system, (2.22), (2.23) and (2.24) or (2.25), for the evolution of small disturbances in a compact form as

$$\frac{\partial}{\partial t}\boldsymbol{A}\tilde{\phi} = \boldsymbol{B}\tilde{\phi}. \tag{2.26}$$

The full expressions of matrices $\boldsymbol{A}$ and $\boldsymbol{B}$ are given in the Appendix.

2.3.1. *Modal and non-modal stability analysis*

For a modal stability analysis we assume an exponential behaviour in time,

$$\phi(x, y, z, t) = \tilde{\phi}(y, t)\mathrm{e}^{\mathrm{i}\alpha x + \mathrm{i}\gamma z} = \hat{\phi}(y)\mathrm{e}^{-\mathrm{i}\omega t}\mathrm{e}^{\mathrm{i}\alpha x + \mathrm{i}\gamma z}, \tag{2.27}$$

and obtain the generalized eigenvalue problem

$$-\mathrm{i}\omega \boldsymbol{A}\hat{\phi} = \boldsymbol{B}\hat{\phi}. \tag{2.28}$$

It is, however, well known that modal analysis fails to predict transition in the case of wall-bounded shear flows. These flows become turbulent at subcritical Reynolds numbers, below the threshold for the occurrence of exponential instability, if any. Non-modal analysis is therefore necessary to investigate the potential for transient energy growth of specific disturbances (e.g. Farrell 1988; Reddy, Schmid & Henningson 1993). This is most readily done by casting the stability problem as an initial value problem, i.e.

$$\frac{\partial}{\partial t}\tilde{\phi} = \boldsymbol{L}\tilde{\phi}, \tag{2.29}$$

where $\boldsymbol{L}$ is the linearized operator obtained by $\boldsymbol{A}^{-1}\boldsymbol{B}$, where $\boldsymbol{A}^{-1}$ is the inverse of the matrix $\boldsymbol{A}$ (see the Appendix).

In our analysis, we consider the flow behaviour in the case where an initial disturbance is added to the fluid velocity only, and we measure the response in terms of flow kinetic energy,

$$E(t) = \frac{1}{2}\int_{\Omega} \phi^{*}\boldsymbol{M}\phi \,\mathrm{d}V, \tag{2.30}$$

where $\boldsymbol{M}$ is the energy weight matrix. Input and output matrices are introduced such that the initial condition is $\phi = \boldsymbol{B}_{in}\phi_{in}$ and the output energy is defined only for $\phi_{out} = \boldsymbol{C}_{out}\phi$. The matrix $\boldsymbol{B}_{in}$ forces the perturbation of the polymer stress to be zero, whereas the matrix $\boldsymbol{C}_{out}$ ensures that only the final energy of the fluid velocity is considered. They are defined as in Klinkenberg, De Lange & Brandt (2011):

$$\boldsymbol{B}_{in} = \begin{pmatrix} 1 & 0 \\ 0 & 1 \\ 0 & 0 \\ 0 & 0 \\ 0 & 0 \\ 0 & 0 \\ 0 & 0 \\ 0 & 0 \end{pmatrix}, \quad \boldsymbol{C}_{out} = \begin{pmatrix} 1 & 0 & 0 & 0 & 0 & 0 & 0 & 0 \\ 0 & 1 & 0 & 0 & 0 & 0 & 0 & 0 \end{pmatrix}. \tag{2.31}$$

The evolution operator from ϕ_{in} to ϕ_{out} becomes $\boldsymbol{T} = \boldsymbol{C}_{out}\mathrm{e}^{t\boldsymbol{L}}\boldsymbol{B}_{in}$ and the input and output energy matrices are decomposed as $\boldsymbol{M}_{in} = \boldsymbol{F}_{in}\boldsymbol{F}_{in}^{*}$ and $\boldsymbol{M}_{out} = \boldsymbol{F}_{out}\boldsymbol{F}_{out}^{*}$ using the Cholesky decomposition. The optimal energy growth in L^2-norm with given input–output is

$$\begin{aligned} G(t) &= \max_{\phi_0} \frac{\|\phi_{out}(t)\|_{Eout}}{\|\phi_{in}(0)\|_{Ein}} = \max_{\phi_0} \frac{\|\boldsymbol{T}\phi_{in}(0)\|_{Eout}}{\|\phi_{in}(0)\|_{Ein}} = \max_{\phi_0} \frac{\|\boldsymbol{F}_{out}\boldsymbol{T}\phi_{in}(0)\|_2}{\|\boldsymbol{F}_{in}\phi_{in}(0)\|_2} \\ &= \max_{\phi_0} \frac{\|\boldsymbol{F}_{out}\boldsymbol{T}\boldsymbol{F}_{in}^{-1}\boldsymbol{F}_{in}\phi_{in}(0)\|_2}{\|\boldsymbol{F}_{in}\phi_{in}(0)\|_2} = \|\boldsymbol{F}_{out}\boldsymbol{T}\boldsymbol{F}_{in}^{-1}\|_2 = \|\boldsymbol{F}_{out}\boldsymbol{C}_{out}\mathrm{e}^{t\boldsymbol{L}}\boldsymbol{B}_{in}\boldsymbol{F}_{in}^{-1}\|_2. \end{aligned} \tag{2.32}$$

As discussed by Doering, Eckhardt & Schumacher (2006), the natural energy of the fluid and the polymer does not correspond to a proper functional norm on perturbations that can be directly used for a non-modal analysis. Using input and

output operators we consider here only the fluid kinetic energy as a measure of the disturbance, as this seems more relevant to transition. More importantly, we introduce a perturbation in the fluid velocity only at the initial time. In other words, the momentum equations are forced by a Dirac delta in time, whereas the polymer stretching is not perturbed directly but only indirectly at $t = 0^+$ via the fluid. This approach is adopted as more natural way to perturb the flow, closest to what can be achieved in an experiment.

2.3.2. *Energy analysis*

The kinetic energy budget provides another approach to analysing the instability mechanisms in polymeric flows (see e.g. Hoda *et al.* 2008, 2009). The hydrodynamic perturbation kinetic energy is obtained by multiplying the linearized equation (2.19) by the complex conjugate of the perturbation velocity:

$$u_i^* \frac{\partial u_i}{\partial t} = -u_i^* U_j \frac{\partial u_i}{\partial x_j} - u_i^* \frac{\partial p}{\partial x_i} + u_i^* \frac{\beta}{Re} \frac{\partial^2 u_i}{\partial^2 x_j} + u_i^* \frac{1-\beta}{Re} \frac{\partial \tau_{ij}}{\partial x_j} - u_i^* u_j \frac{\partial U_i}{\partial x_j}. \tag{2.33}$$

Taking the complex conjugate of the above equation and adding the two equations, we obtain

$$\begin{aligned} \frac{\partial (e)}{\partial t} = & -\frac{\beta}{Re} \frac{\partial u_i^*}{\partial x_j} \frac{\partial u_i}{\partial x_j} - \frac{1-\beta}{2Re} \left(\tau_{ij} \frac{\partial u_i^*}{\partial x_j} + \tau_{ij}^* \frac{\partial u_i}{\partial x_j} \right) - \frac{1}{2} \left(u_i^* u_j \frac{\partial U_i}{\partial x_j} + u_i u_j^* \frac{\partial U_i}{\partial x_j} \right) \\ & + \frac{\partial}{\partial x_j} \left[-\frac{1}{2} u_i u_i^* U_j - \frac{1}{2} (u_i p^* + u_i^* p) \delta_{ij} \right. \\ & \left. + \frac{\beta}{2Re} \left(u_i^* \frac{\partial u_i}{\partial x_j} + u_i \frac{\partial u_i^*}{\partial x_j} \right) + \frac{1-\beta}{2Re} (u_i^* \tau_{ij} + u_i \tau_{ij}^*) \right], \end{aligned} \tag{2.34}$$

where $e(y, t) = u_i^* u_i / 2$ is the perturbation energy density. The terms in the square brackets are transport terms which only redistribute the energy inside the domain. Thus, if the boundary conditions are homogeneous or periodic, these transport terms do not contribute to the net variation of the energy density. Integrating the above equation in space, we obtain

$$\begin{aligned} \int_{-1}^{1} \frac{\partial (e)}{\partial t} \, \mathrm{d}y = & - \int_{-1}^{1} \frac{1}{2} (u_i^* u_j + u_i u_j^*) \frac{\partial U_i}{\partial x_j} \, \mathrm{d}y \\ & - \int_{-1}^{1} \frac{1-\beta}{2Re} \left(\tau_{ij} \frac{\partial u_i^*}{\partial x_j} + \tau_{ij}^* \frac{\partial u_i}{\partial x_j} \right) \mathrm{d}y - \int_{-1}^{1} \frac{\beta}{Re} \frac{\partial u_i^*}{\partial x_j} \frac{\partial u_i}{\partial x_j} \, \mathrm{d}y. \end{aligned} \tag{2.35}$$

The first term on the right-hand side indicates the production of the Reynolds stresses against the shear of the base flow and it is responsible for the instability in Newtonian fluids. This will be denoted Pr in the following and reduces to $-(1/\Omega) \int_\Omega ((u_1^* u_2 + u_1 u_2^*)/2)(\partial U / \partial x_2) \, \mathrm{d}V$ for a parallel base flow. The second term, denoted PD, indicates the rate of work of the polymeric stresses, in other words the energy exchanged in the interaction between the polymer fluctuating stress field and the fluctuating flow field. The last term on the right-hand side represents viscous dissipation and it is strictly negative. This will be denoted VD, with subscripts if necessary. For example, VD_{11} refers to $-(1/\Omega) \int_\Omega (\beta/Re)(\partial u_1^* / \partial x_1)(\partial u_1 / \partial x_1) \, \mathrm{d}V$ (similarly for the other terms).

Finally, note that for normal modes, the normalized time variation of the energy density R_e can be written as

$$R_e = \frac{\dfrac{1}{\Omega}\displaystyle\int_\Omega \frac{\partial(e)}{\partial t}\,\mathrm{d}V}{\dfrac{1}{\Omega}\displaystyle\int_\Omega e\,\mathrm{d}V} = 2\omega_i, \tag{2.36}$$

where ω_i is the imaginary part of the eigenvalue whose eigenfunction is used to evaluate the production and dissipation terms. This expression can be used as an *a posteriori* check of the results.

3. Numerical methods and validation

To solve the equations introduced above, we use a spectral collocation method based on Chebyshev modes. The original Chebyshev polynomials have been modified to directly account for boundary conditions by adding the prefactor (Weideman & Reddy 2000; Canuto *et al.* 2007)

$$L_j^+(y) = \left(\frac{1-y^2}{1-y_j^2}\right)^2 L_j(y) \tag{3.1}$$

and

$$L_j^+(y) = \left(\frac{1-y^2}{1-y_j^2}\right) L_j(y) \tag{3.2}$$

for the Orr–Sommerfeld and Squire problems respectively.

As mentioned before, we wish to solve a linear system, $\boldsymbol{A}(\partial/\partial t)\phi = \boldsymbol{B}\phi$, where ϕ is $(v, \eta, c_{11}, c_{22}, c_{33}, c_{12}, c_{13}, c_{23})^{\mathrm{T}}$. The matrices $\boldsymbol{A}$ and $\boldsymbol{B}$ are of size $(8N+12)\times(8N+12)$ in three dimensions, where v and η are approximated by N modes whereas each component of the conformation tensor c_{ij} is approximated by $N+2$ modes. Left-multiplying by $\boldsymbol{A}^{-1}$ and using the assumption of exponential behaviour in time, we obtain $\omega\hat{\phi}(y) = \mathrm{i}\boldsymbol{A}^{-1}\boldsymbol{B}\hat{\phi}(y)$, where ω is the eigenvalue and $\hat{\phi}(y)$ is the eigenfunction. The non-modal analysis is performed by computing the singular value decomposition of the matrix exponential $\exp(t\boldsymbol{A}^{-1}\boldsymbol{B})$. The parameter space to be investigated is defined by $(\alpha, \gamma, W, Re, \beta, L)$.

3.1. *Validation*

The implementation of the Oldroyd-B fluid is validated against the results by Sureshkumar & Beris (1995). In table 1 we compare the results from this previous work and the present implementation for Poiseuille flow of the Oldroyd-B fluid at $Re = 3960$, $\beta = 0.5$, $W = 3.96$, $\alpha = 1.15$, $\gamma = 0$. The critical eigenvalue is in good agreement when using 129 Chebyshev modes in our implementation.

The implementation of the FENE-P model is expected to generate the same eigenspectrum as the Oldroyd-B model when $L \gg 1$ and the other parameters the same. This is verified for $Re = 3960$, $\beta = 0.5$, $W = 3.96$, $\alpha = 1.15$, $\gamma = 0$ and $L = 10\,000$. The number of modes used in the discretization is 101 for v and η and 103 for each component of c_{ij}. As we could not find results in the literature for the FENE-P flow at high Reynolds numbers, we verify the current implementation by comparison to the energy budget (see (2.36) and results below.)

	Present implementation	Sureshkumar & Beris (1995)
Critical eigenvalues	$0.34089441 + 1.9888 \times 10^{-7}\mathrm{i}$	$0.34089442 + 1.9696 \times 10^{-7}\mathrm{i}$

TABLE 1. Validation of the Oldroyd-B implementation against the results in Sureshkumar & Beris (1995). Least stable mode for $Re = 3960$, $\beta = 0.5$, $W = 3.96$, $\alpha = 1.15$, $\gamma = 0$.

For the majority of the results, we used 131 grid points for the flow variables and 133 for each component of the polymer conformation tensor. Table 2 demonstrates that the results are resolution-independent.

4. Modal stability of viscoelastic channel flow

When evaluating neutral stability curves, we focus only on two-dimensional disturbances and compare the results of a FENE-P fluid to Newtonian and Oldroyd-B fluids. As shown by Bistagnino *et al.* (2007), Squire's theorem can be extended to Oldroyd-B fluids and it is therefore sufficient to consider two-dimensional waves to determine the critical Reynolds number. However, owing to the coupling induced by the FENE function, a similar extension might not be possible for FENE-P fluids. Hence, we analysed three-dimensional modes for different values of γ and α and found that the two-dimensional waves appear to be the first to become unstable also with the FENE-P closure.

Neutral curves of FENE-P fluid in the (α, Re) plane are depicted in figure 2(*a*) for different values of the Weissenberg number, W, and for $\beta = 0.9$, $L = 60$ and $\gamma = 0$. For large W, the strong elastic effect stabilizes the flow. Interestingly, at smaller W ($W \approx 1$), the flow appears to be less stable (note that the Reynolds number is defined using the total fluid viscosity). The non-monotonic behaviour of the critical Reynolds number in polymeric flows has been previously observed in the studies by Sadanandan & Sureshkumar (2002), Stone *et al.* (2004) and Roy *et al.* (2006). We will discuss this in detail in connection with figure 3 and when performing an energy budget analysis. Figure 2(*b*) shows the effect of the viscosity ratio β on the neutral stability curve at $W = 10, L = 60, \gamma = 0$. Decreasing β (increasing the polymer concentration), the critical Reynolds number increases, i.e. at this relatively large W, stronger elasticity stabilizes the flow. For values of $\beta < 0.5$ (not shown here), the results of the modal analysis are found to be almost independent of β and the critical Reynolds number is approximately 8300, and it occurs for a streamwise wavenumber slightly larger than for the Newtonian counterpart, $\alpha \approx 1.05$.

The critical Reynolds number is shown versus the non-dimensional relaxation time $W\omega_r$ in figure 3 for different values of β and for the two models, FENE-P and Oldroyd-B. The frequency ω_r is the real part of the least stable eigenvalue (the frequency of the disturbance) at the critical condition, so that $W\omega_r$ is the polymer relaxation time over the period of the marginally stable wave. The critical values of Re are obtained by searching for a minimum in the (α, Re) plane for each case, so that α is in general different for each point in figure 3. In all cases, the critical Reynolds number first decreases and reaches its minimum at $W\omega_r \approx 1$ before increasing. Higher critical Re indicates a more stable flow when the polymer relaxation times becomes

Modes	Oldroyd-B	FENE-P ($L = 60$)
32	$0.341234084409063 - 0.000323777796261\mathrm{i}$	$0.343564949051865 - 0.002229595239572\mathrm{i}$
65	$0.340894448265977 + 0.000000297308649\mathrm{i}$	$0.343253495595805 - 0.001933245318672\mathrm{i}$
131	$0.340894410778315 + 0.000000198881448\mathrm{i}$	$0.343253443294946 - 0.001933260576780\mathrm{i}$
258	$0.340894410782048 + 0.000000198877210\mathrm{i}$	$0.343253443295637 - 0.001933260579580\mathrm{i}$

TABLE 2. Resolution check at $Re = 3960$, $\beta = 0.5$, $W = 3.96$, $\alpha = 1.15$, $\gamma = 0$ for Oldroyd-B and for FENE-P fluid with $L = 60$.

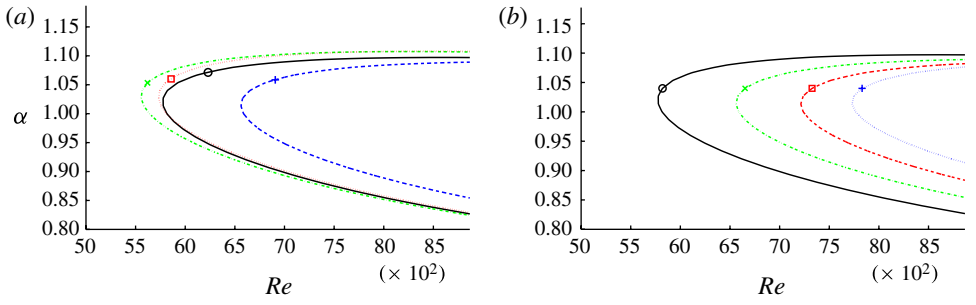

FIGURE 2. (Colour online) (*a*) Neutral curves at $\beta = 0.9, L = 60, \gamma = 0$ and $W = 0$ (Newtonian, ◯), $W = 1$ (×), $W = 5$ (□), $W = 10$ (+). (*b*) Neutral curves at $W = 10, L = 60, \gamma = 0$ and $\beta = 1$ (Newtonian, ◯), $\beta = 0.9$ (×), $\beta = 0.8$ (□), $\beta = 0.7$ (+).

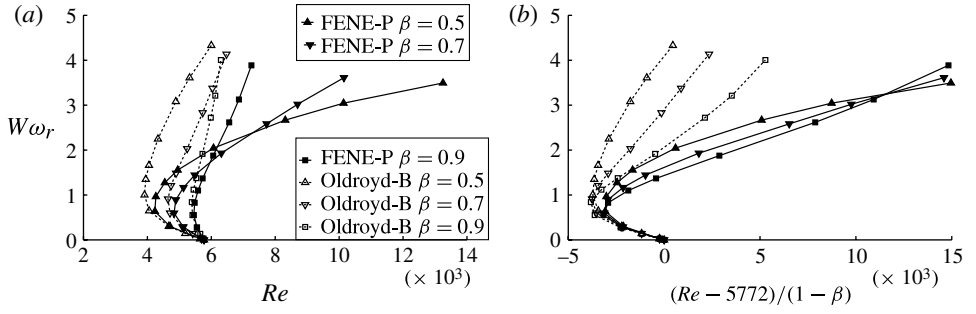

FIGURE 3. (*a*) Neutral curves versus $W\omega_r$ and Re for $L = 60$, $\gamma = 0$, and $\beta = 0.5$ (−−△−−), $\beta = 0.7$ (−−▽−−), $\beta = 0.9$ (−−□−−) for Oldroyd-B model, and $\beta = 0.5$ (−▲−), $\beta = 0.7$ (−▼−), $\beta = 0.9$ (−■−) for FENE-P model. (*b*) Neutral curves versus $(Re - 5772)/(1 - \beta)$ for $L = 60$, $\gamma = 0$; symbols as in (*a*).

longer than the instability time scale. One can also note from the figure that at large W the flow modelled by the FENE-P closure is more stable for lower β.

Interestingly, at lower $W\omega_r$, the curves for different β values collapse into a single curve once we plot the marginal condition versus the abscissa $(Re - 5772)/(1 - \beta)$, as shown in figure 3(*b*). This implies that the deviations from the Newtonian critical limit ($Re = 5772$) are proportional to the polymer viscosity ($Re/(1 - \beta) = \rho U_c L_c/\mu_p$). Energy analysis will help shed some light onto this effect as well as onto the stabilization observed at high $W\omega_r$.

We summarize in figure 4 the variation of the critical Reynolds number versus W and β. The black line is the iso-level corresponding to the critical Re for the Newtonian case, $Re = 5772$. With decreasing β, the destabilization effect at small W is more apparent. The highest critical Re is expected to be found in the top left corner, where the elasticity is strongest.

The effect of L is displayed in figure 5 for the viscosity ratio $\beta = 0.9$. The Oldroyd-B model can be seen as the limit of the FENE-P results when $L \to \infty$, and indeed the result of the Oldroyd-B model appears as the limit of the series of results for the FENE-P model with increasing L. The smaller L suppresses the maximum possible extension of the polymer molecules. The data clearly indicate that

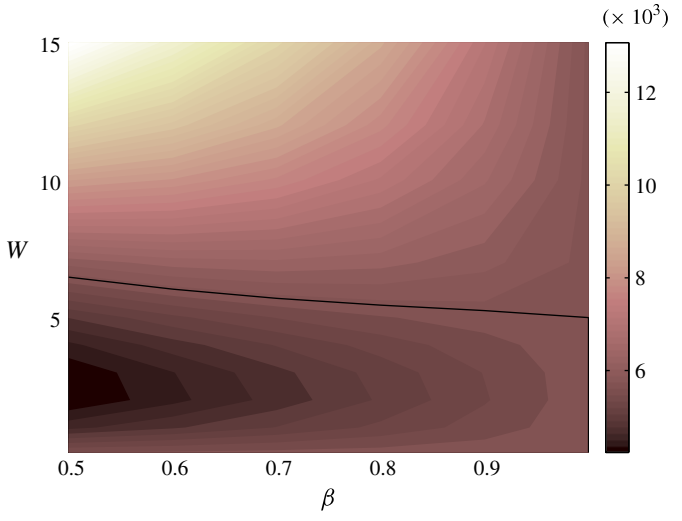

FIGURE 4. (Colour online) Critical Reynolds number in the (β, W) plane for a FENE-P fluid with $L = 60$.

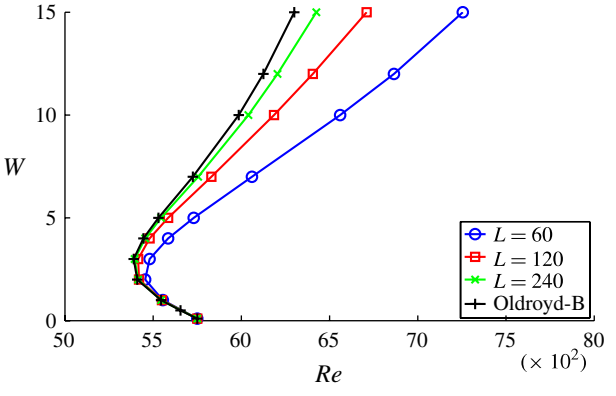

FIGURE 5. (Colour online) Neutral curves at $\beta = 0.9$, $\gamma = 0$, and $L = 60$ (◯, blue), $L = 120$ (□, red), $L = 240$ (×, green) in FENE-P model; Oldroyd-B model (+, black).

fluids characterized by a smaller value of the maximum extensibility L are always the most stable. By examining the base flow conformation tensor C_{kk}, we see that the strongest stabilization is observed when the polymers are already significantly stretched (∼60 % of the maximum). This is in agreement with the observations of maximum stabilization at large W discussed earlier, when the trace of the conformation tensor also reaches values larger than $0.5\ L^2$.

4.1. *Energy analysis*

Table 3 reports the energy budget at $\beta = 0.7$, $Re = 5300$, $L = 60$, $\alpha = 1.02$, $\gamma = 0$, where $W = 0$ corresponds to the Newtonian flow. The results have all been normalized by the integral of the perturbation energy density. The total time variation of energy

Terms ($\times 10^{-4}$)	$W=0$	$W=0.5$	$W=2.5$	$W=10$
PD_{11}	0	−4.306	−9.058	178.058
PD_{12}	0	−41.351	−38.207	−177.607
PD_{21}	0	0.488	0.078	−1.281
PD_{22}	0	−1.720	−1.946	−2.234
VD_{11}	−2.824	−1.977	−1.978	−1.999
VD_{12}	−145.152	−101.974	−104.951	−138.212
VD_{21}	−1.102	−0.771	−0.770	−0.749
VD_{22}	−2.824	−1.977	−1.978	−1.999
PD	0	−46.890	−49.132	−3.065
VD	−151.902	−106.699	−109.678	−142.959
Pr	134.230	147.678	173.622	42.885
Total	−17.672	−5.911	14.811	−103.139
$2\omega_i$	−17.672	−5.911	14.811	−103.139

TABLE 3. Energy budget for modal instability of viscoelastic Poiseuille flow for different values of the Weissenberg number. $\beta=0.7$, $Re=5300$, $L=60$, $\alpha=1.02$, $\gamma=0$. $W=0$ corresponds to Newtonian flow. Note that the data in the table have been divided by 10^{-4}.

Terms ($\times 10^{-4}$)	$L=60$	$L=120$	$L=500$
PD_{11}	3.416	3.621	3.745
PD_{12}	−16.412	−16.978	−17.202
PD_{21}	−0.260	−0.286	−0.296
PD_{22}	−0.669	−0.689	−0.696
VD_{11}	−2.408	−2.408	−2.408
VD_{12}	−131.730	−131.746	−131.779
VD_{21}	−0.936	−0.937	−0.937
VD_{22}	−2.408	−2.408	−2.408
PD	−13.925	−14.333	−14.449
VD	−137.482	−137.498	−137.530
Pr	140.032	147.161	149.969
Total	−11.375	−4.670	−2.010
$2\omega_i$	−11.375	−4.670	−2.010

TABLE 4. Energy budget for modal instability of viscoelastic Poiseuille flow for different values of the maximum length $L\beta=0.9$, $W=6$, $Re=5600$, $\alpha=1.02$, $\gamma=0$. Note that the data in the table have been divided by 10^{-4} .

density is the sum of PD, VD and Pr, and this corresponds to $2\omega_i$ (see (2.36)), where ω_i is the imaginary part of the least stable eigenvalue, as confirmed in the table.

The total dissipation, which is the sum of the viscous dissipation and the negative rate of polymer work, is almost constant for different W. When the rate of polymer work decreases, the viscous dissipation increases and vice versa. At low W, the critical Reynolds number decreases where this enhanced instability of the flow is dictated by an increase in the production due to the uv Reynolds stress against the base flow shear. In the same way, at large W, the flow is stabilized because the same production term is now decreasing.

The energy budget when changing the maximum admissible polymer extension L is presented in table 4 for $\beta=0.9, W=6, Re=5600, \alpha=1.02, \gamma=0$. The data reveal

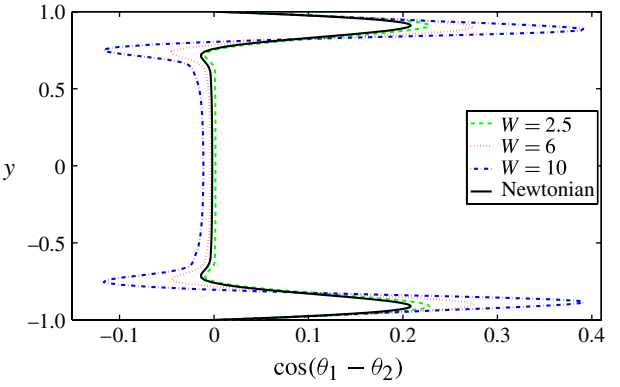

FIGURE 6. (Colour online) Wall-normal distribution of the phase difference $\cos(\theta_1 - \theta_2)$ between streamwise and wall-normal components of the least stable eigenmode: Newtonian, (−, black), $W = 2.5$ (- -, green), $W = 6$ (. . ., red), $W = 10$ (-·-·-, blue).

that the total production against the mean shear, Pr, increases with increasing L while the negative terms, PD and VD are almost independent of L. This explains why larger values of the extensibility L lead to a more unstable flow, as shown in figure 5.

The cosine of the phase difference between the streamwise and wall-normal components of the eigenfunction is shown in figure 6. This phase difference, induced by the viscosity, is known to be responsible for the positive production term Pr leading to the viscous instability in channel flow of Newtonian fluids (Huerre & Rossi 1998). This phase difference explains why inviscid flows without an inflection point are unstable in the presence of viscosity: a 90° phase difference, as in neutrally stable inviscid flows, would give zero production. The phase difference (and therefore the production against the mean shear) is generated in a region near the wall, the critical layer, whereas it is almost zero in the bulk of the flow. Increasing W creates a large region of negative production just above the critical layer while also increasing the peak of positive production. When the former effect is stronger, $W\omega_r \gtrsim 1$, the total production is less and the flow is more stable (see figure 2*a*).

In summary, the results of modal stability demonstrate that the production of disturbance kinetic energy increases at $W\omega_r \lesssim 1$ when the polymer relaxation time is shorter than the instability time scale, and therefore polymer molecules do not stretch significantly more than in the base configuration. In this range, the total dissipation is almost constant and equal to the Newtonian value for the same total viscosity: the polymers are almost inelastic and the polymer work rate is proportional to viscous dissipation (see also Zhu, Lauga & Brandt 2011). The destabilization is therefore explained by an increasing viscous production ($|uv|\cos(\theta_1 - \theta_2)$), as the polymer viscosity alters the time delay between the streamwise and wall-normal velocity perturbations. This observation is also consistent with the results in figure 3(*b*), where the destabilization is shown to be proportional to the polymer viscosity. The most unstable cases, or the lowest critical Reynolds numbers, are found when $W\omega_r \approx 1$, before the perturbation kinetic energy production decreases for $W\omega_r \gtrsim 1$ when the polymer has time to stretch further with respect to the base flow configuration. The critical Reynolds number then increases and we observe a significant stabilization, again proportional to the polymer viscosity for the FENE-P fluid (cf. figure 3*b*).

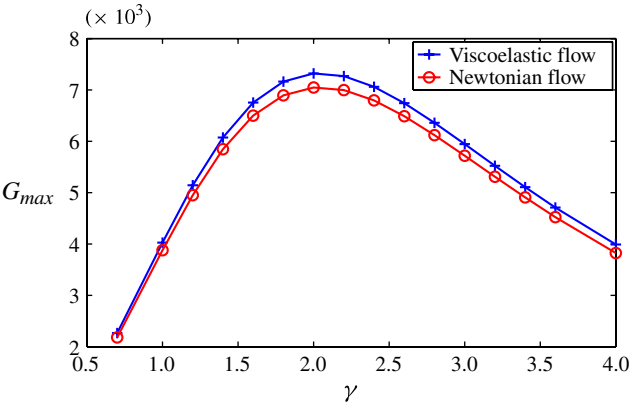

FIGURE 7. (Colour online) Overall amplification G_{max} versus the spanwise wavenumber γ of disturbances with $\alpha = 0$ for viscoelastic flow (+; $L = 60$, $\beta = 0.9$, $Re = 6000$, $W = 10$) and Newtonian flow (◯).

5. Non-modal stability

The non-modal linear stability analysis of non-Newtonian–Poiseuille flow has not been explored extensively until recently. Doering *et al.* (2006) reported the non-modal amplification of the perturbations in Oldroyd-B fluids at low Reynolds and high Weissenberg numbers, and concluded that while a base flow may be linearly stable, the extra degrees of freedom in the polymers may allow for exact solutions displaying non-normal transient growth. Hoda *et al.* (2008, 2009) analysed the energy density of the Oldroyd-B Poiseuille flow. These authors found significant energy amplification also under the action of elasticity. In this section we aim to investigate the transient disturbance growth in Poiseuille flow modelled by the FENE-P closure as well as Oldroyd-B and Newtonian fluids for comparison in the inertial regime. As mentioned in § 2, only the fluid velocity perturbation is considered in this study, and the response only concerns the fluid kinetic energy. Note that when showing results for different fluids, we assume that flows are driven by the same pressure gradient.

In figure 7 we display the overall maximum growth G_{max}, the maximum over all possible final times, for different γ and $L = 60$, $\beta = 0.9$, $W = 10$, $Re = 6000$, $\alpha = 0$, together with the results for Newtonian flow. The case with streamwise wavenumber $\alpha = 0$ is of particular interest because this combination ($\alpha = 0, \gamma = 2$) gives the global maximum in the wavenumber space for Newtonian fluids (Schmid & Henningson 2001); and for viscoelastic fluids as shown here. To simplify the presentation of the results and the corresponding analysis, we therefore consider disturbances for a fixed spanwise wavenumber $\gamma = 2$, and vary the streamwise wavelength and the rheological parameters.

Note that we obtain the optimal growth and initial condition from the singular value decomposition of the matrix $\boldsymbol{L}$. The initial condition is the left singular vector corresponding to the largest singular value of the matrix. The optimal initial condition and response are reported in figure 8 for a viscoelastic fluid with $L = 60, \beta = 0.9, W = 10, Re = 6000, \alpha = 0, \gamma = 2$. The figure demonstrates that the lift-up mechanism is still at work in viscoelastic fluids, as in the Newtonian case. The optimal initial condition consists of counter-rotating streamwise vortices, in particular one vortex across the channel cross-section, whereas the final response is

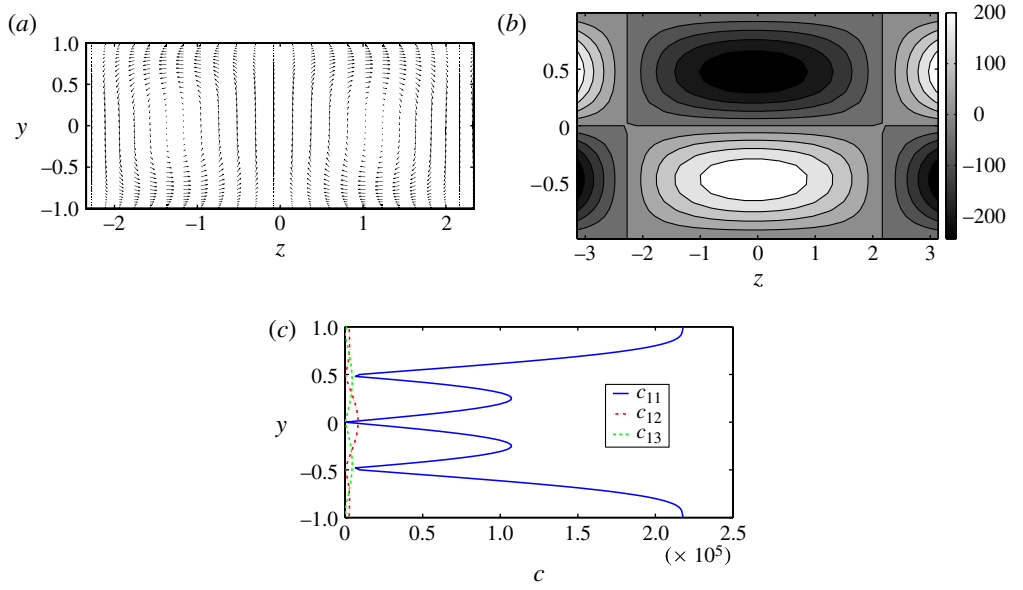

FIGURE 8. (Colour online) (*a*) Velocity vectors in the cross-stream plane of the optimal initial condition, (*b*) the streamwise velocity component of the optimal response and (*c*) polymeric stresses at the time of optimal growth in viscoelastic flow with $L = 60$, $\beta = 0.9$, $W = 10$, $Re = 6000$, $\alpha = 0$, $\gamma = 2$.

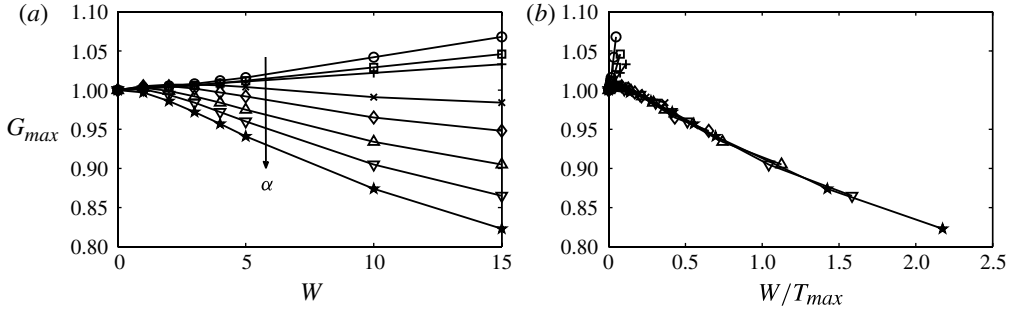

FIGURE 9. Transient growth versus the Weissenberg number, W, for viscoelastic fluid with $L = 60$, $\beta = 0.9$, $Re = 4000$, $\gamma = 2$ and different values of the streamwise wavenumber: $\alpha = 0$ (◯), $\alpha = 0.05$ (□), $\alpha = 0.1$ (+), $\alpha = 0.5$ (×), $\alpha = 1.02$ (◇), $\alpha = 2$ (△), $\alpha = 3$ (▽), $\alpha = 4$ (⋆).

characterized by a large streamwise perturbation velocity, with positive and negative regions alternating in the spanwise direction, the so-called streamwise streaks, arranged in a staggered array in the wall-normal direction. The elastic stress at the time of maximum energy amplification is displayed in figure 8(*c*). The τ_{11} component has increased dramatically when compared to the other stress components.

Figure 9(*a*) shows how viscoelasticity affects the transient growth for $L = 60$, $\beta = 0.9$, $Re = 4000$, $\gamma = 2$ when varying the streamwise wavenumber of the perturbation. The data are normalized with respect to the Newtonian value of $G_{max}(W = 0)$ for each

	$W=0$	$W=0.5$	$W=1$	$W=1.5$	$W=5$	$W=10$	$W=15$
$\alpha=0$	3135.42	3138.45	3142.11	3138.50	3183.18	3263.52	3345.28
$\alpha=1.02$	406.65	407.33	407.48	407.33	401.86	391.24	384.31
$\alpha=2$	137.12	137.16	136.96	137.16	133.32	127.66	123.65
$\alpha=4$	26.26	26.18	26.05	26.18	24.72	22.94	21.62

TABLE 5. Optimal growth G_{max} for different values of the Weissenberg number and of the streamwise wavenumber α. $L=60$, $\beta=0.9$, $Re=4000$, $\gamma=2$. The data are displayed in figure 9.

α. Note that the optimal transient growth decreases when increasing the streamwise wavenumber (first column in table 5).

For small α, G_{max} increases monotonically when increasing W. This increase, although somewhat limited to a few per cent, was also documented by Hoda *et al.* (2008). Increasing α, the maximum amplification, G_{max}, increases slightly for $W \lesssim 1$ where the elastic effect of polymer molecules is still weak, and then decreases when W is increased further. Polymers with large enough W therefore have a stabilizing effect on oblique travelling modes. When λ is small, the polymer molecules react very rapidly to the wave propagating in the flow without manifesting their elasticity. On the other hand, when λ is large, the polymer molecules stay stretched for a longer period and the level of interaction with the fluid increases. The perturbation energy will be absorbed by these polymers with large W (stored as elastic energy), leading to a more stable flow.

We display the same data in figure 9(*b*), where the polymer relaxation time is scaled by the time T_{max} corresponding to the largest possible amplification. Here, we find that all curves pertaining to disturbances with finite values of $\alpha > 0.1$ collapse onto a single curve. For travelling disturbances, as for the case of modal stability, we see that stabilization occurs when the polymer relaxation time is of the order of, or longer than, the time scale of the instability.

The influence of the viscosity ratio β on the optimal disturbance growth is presented in figure 10. For disturbances with $\alpha=0$, small β yields larger transient growth while for $\alpha=1.02$ and $\alpha=2$ we observe a reduction of the transient growth. In the figure, we display the variation of the optimal growth with respect to the Newtonian case versus the polymer viscosity: the variation is almost linear with β, especially at lower α, i.e. proportional to the polymer viscosity.

The optimal growth for fluids characterized by different values of the maximum extensibility L is displayed in figure 11 for $\alpha=0$, $\alpha=1.02$ and $\alpha=2$. Results are normalized with respect to the growth in the corresponding Newtonian flow. The normalized transient growth decreases with L and asymptotically approaches the result for Oldroyd-B fluid. This marginal variation with L can probably be explained by the particular initial condition used, with no perturbation in the polymer conformation tensor. In more elastic flows, large L, polymers need more time to stretch initially, and this delays the disturbance growth. Note finally that the main features of the transient growth, such as the time of maximum amplification, are not affected by the polymer extensibility and viscosity ratio.

The dependence of the transient growth on the Reynolds number Re is also investigated. Note that Re in the polymer solution is based on the total viscosity and therefore describes the property of the entire solution. In Newtonian flows, the maximum transient growth is proportional to Re^2 (Schmid & Henningson 2001).

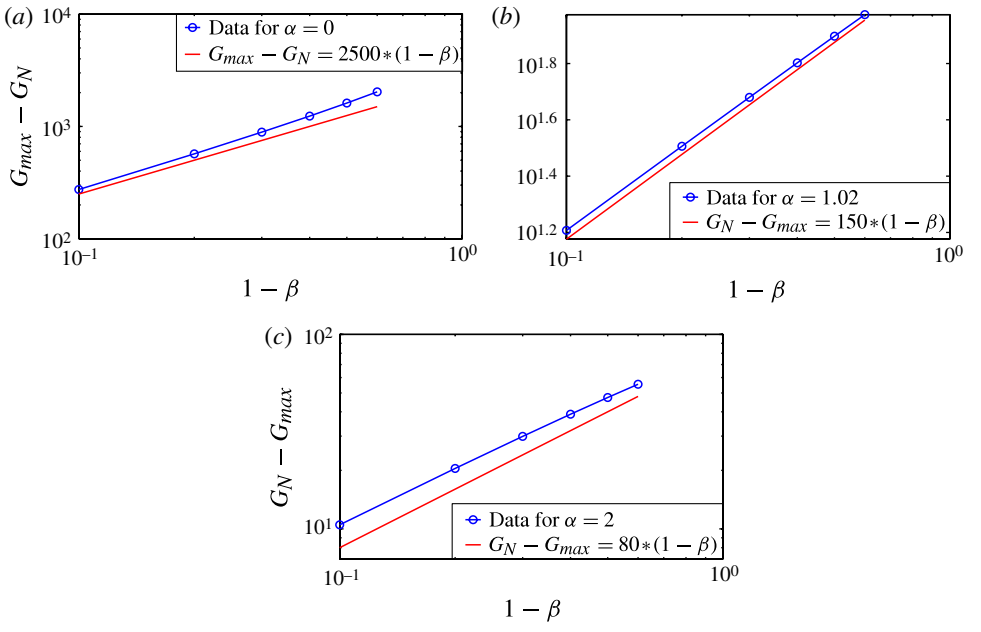

FIGURE 10. (Colour online) Transient growth versus the viscosity ratio β for $W = 10$, $L = 60$, $Re = 6000$, $\gamma = 2$. The global maximum amplification G_{max} versus $1 - \beta$ for increasing values of the streamwise wavenumber α: $\alpha = 0$ (*a*), $\alpha = 1.02$ (*b*), $\alpha = 2$ (*c*). G_N indicates the maximum transient growth for Newtonian flow.

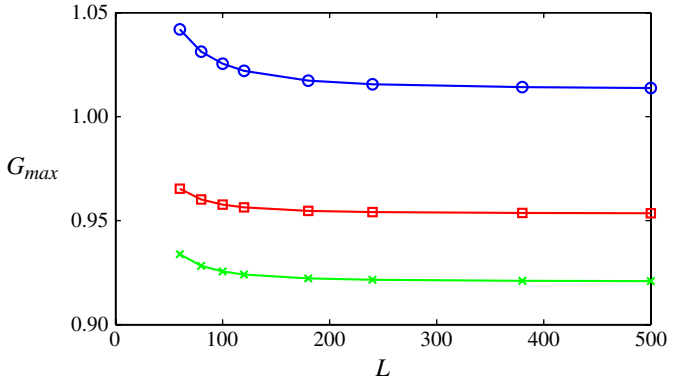

FIGURE 11. (Colour online) Maximum growth divided by the corresponding Newtonian value versus the polymer maximum extensibility L for $W = 10$, $Re = 4000$, $\beta = 0.5$, $\gamma = 2$, and $\alpha = 0$ (◯), $\alpha = 1.02$ (□), $\alpha = 2$ (×).

This is confirmed for viscoelastic fluids in figure 12(*a*), where the optimal growth is depicted in logarithmic scale for disturbances with $\alpha = 0$. Here one can also note that G_{max} is larger in the polymer solution. For oblique modes with $\alpha = 1.02$ (see figure 12*b*), the global maximum amplification is linearly proportional to Re, as for Newtonian fluids. In this case, G_{max} is instead larger for Newtonian fluids. In addition,

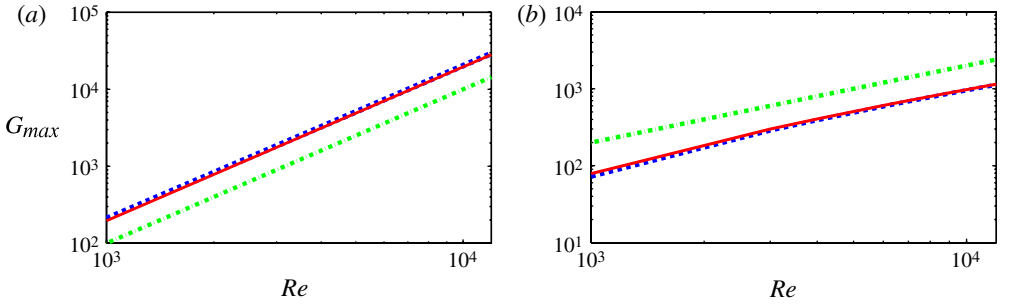

FIGURE 12. (Colour online) Global maximum of non-modal amplification G_{max} versus the Reynolds number Re for $\beta = 0.9, L = 60, W = 10, \gamma = 2$. ($a$) $\alpha = 0$: viscoelastic flow (- -, blue), Newtonian flow (–, red), $Re^2/10^4$ (-.-., green). (b) $\alpha = 1.02$: viscoelastic flow (- -, blue), Newtonian flow (–, red), $Re/5$ (-.-., green).

we report that the time of maximum growth is a linear function of Re, also in agreement with the findings for Newtonian fluids.

5.1. *Energy analysis*

The energy budget is examined in order to gain more insight into the effect of polymers on the non-modal amplification of streaks and oblique disturbances. The latter, although characterized by lower linear amplification, are fundamental for the final stages of breakdown to turbulence as well as for transition initiated by localized disturbances or by nonlinear interactions of weak disturbances, for example in oblique transition scenarios (Berlin, Lundbladh & Henningson 1994), which is found to be the most efficient in canonical shear flows (Duguet, Brandt & Larsson 2010).

We consider the flow kinetic energy in physical space (Butler & Farrell 1992) and write an evolution equation for ϵ,

$$\begin{aligned}\dot{\epsilon} &= \frac{1}{\Omega}\int_{-1}^{1}\int_{0}^{a}\int_{0}^{b}\frac{\partial}{\partial t}\left(\frac{u^2+v^2+w^2}{2}\right)\mathrm{d}V \\ &= \frac{1}{\Omega}\int_{-1}^{1}\int_{0}^{a}\int_{0}^{b}-uv\frac{\mathrm{d}U}{\mathrm{d}y}-\frac{\beta}{Re}\frac{\partial u_i}{\partial x_j}\frac{\partial u_i}{\partial x_j}-\frac{1-\beta}{Re}\tau_{ij}\frac{\partial u_i}{\partial x_j}\,\mathrm{d}z\,\mathrm{d}x\,\mathrm{d}y,\end{aligned} \tag{5.1}$$

where $\Omega = 2ab$, $a = 2\pi/\alpha$ and $b = 2\pi/\gamma$. The interaction of the flow disturbances with the mean flow-shear and the polymer stress are captured by the terms $-uv(\mathrm{d}U/\mathrm{d}y)$ and $-((1-\beta)/Re)\tau_{ij}(\partial u_i/\partial x_j)$, respectively.

The oblique wave ($\alpha = 2, \gamma = 2$) and the streamwise invariant wave ($\alpha = 0, \gamma = 2$) are investigated for $Re = 2000$, $\beta = 0.5$ and $W = \{0, 1, 12\}$. The results for the oblique disturbance in a Newtonian fluid are shown in figure 13(a). According to Farrell & Ioannou (1993), the Orr mechanism and vortex tilting are simultaneously present for an intermediate ratio of spanwise to streamwise wavenumber in Newtonian flow. For viscoelastic flow with small Weissenberg number ($W = 1$), the results are shown in figure 13(b), where D denotes the sum of the PD and VD in viscoelastic flow and $VD(N)$ is the viscous dissipation in Newtonian flow (where the PD term is zero). Comparing the results for Newtonian fluid with the case $W = 1$ we see that D is close to $VD(N)$ and the production terms are quantitatively similar, indicating that at small W, the polymer molecules behave like the fluid and the elastic effect is negligible. However, with increasing W, the elastic effect becomes relevant and the results in

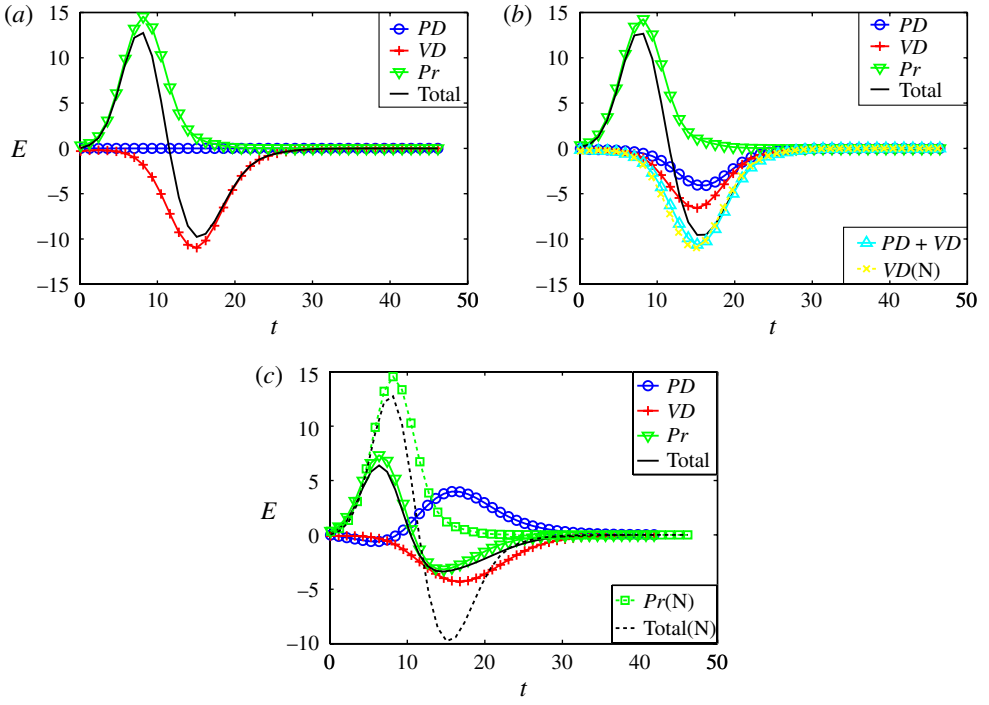

FIGURE 13. (Colour online) Time evolution of the different terms in the energy budget of the optimal disturbance for channel flow at $Re = 2000$, $\beta = 0.5$, $\alpha = 2$, $\gamma = 2$. (*a*) Newtonian: *PD* (◯), *VD* (+), *Pr* (▽), total (−) (*b*) $W = 1$: *PD* (◯), *VD* (+), *Pr* (▽), total (−), *PD* + *VD* (△), *VD* (Newtonian) (×). (*c*) $W = 12$: *PD* (◯), *VD* (+), *Pr* (▽), total (−), *Pr* (Newtonian) (□), total (Newtonian) (- - -).

figure 13(*c*) show that the production is decreasing in viscoelastic fluids, as observed for modal stability in § 4. Although the rate of polymer work becomes positive at later times, $t > 15$, this effect is balanced by an increased viscous dissipation. In summary, the decreased production against mean shear explains the observed reduction in transient growth. From a physical point of view, the mechanism seems similar to that observed for exponentially growing Tollmien–Schlichting waves.

For streamwise independent disturbances, the time evolution of the kinetic energy budget is shown in figure 14(*a*) for Newtonian fluid, and in figure 14(*b,c*) for polymeric fluids with $W = 1$ and $W = 12$. The results for the lowest $W = 1$ in figure 14(*b*) are again similar to those for the Newtonian flow if we consider the sum of *PD* and *VD* (*D* in the figure) in non-Newtonian flow versus the viscous dissipation *VD* in Newtonian flow. The values of the production against the mean shear are also similar. In the case of large polymer relaxation times, $W = 12$ (see figure 14*c*), the production against the mean shear increases and this explains the weak increase of the streak amplification found previously, e.g. figure 9.

6. Discussion and conclusions

We have examined the linear stability of inertia-dominated channel flow of a viscoelastic fluid modelled by the Oldroyd-B and FENE-P models. We performed both modal and non-modal analyses and examined the kinetic energy budget to identify

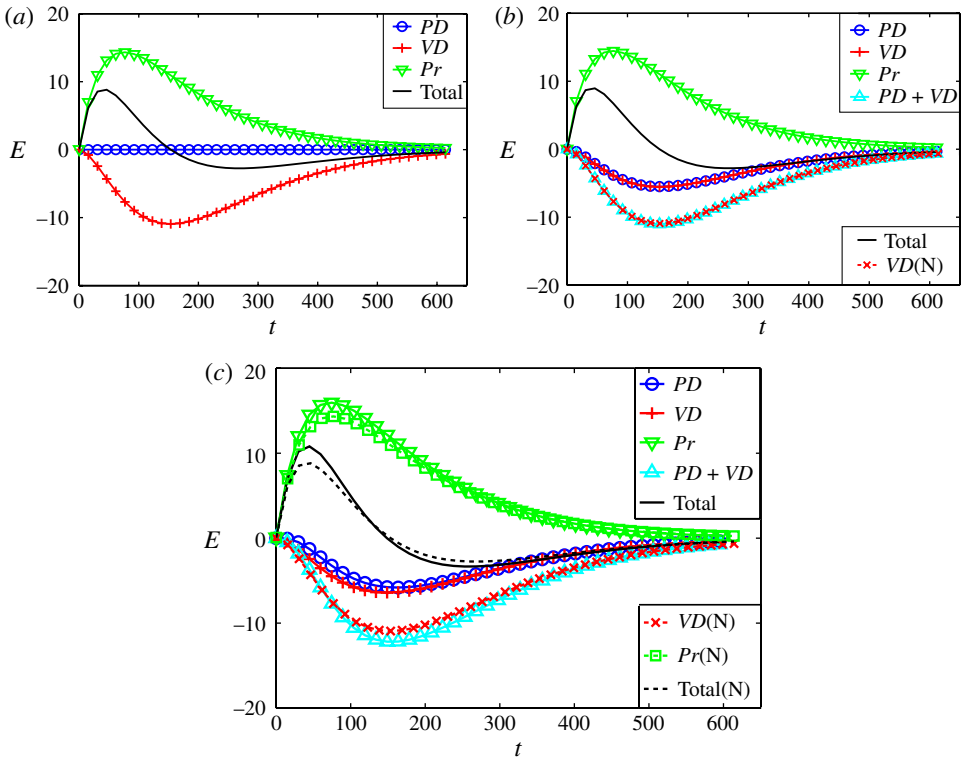

FIGURE 14. (Colour online) Time evolution of the different terms in the energy budget of the optimal disturbance for channel flow at $Re = 2000$, $\beta = 0.5$, $\alpha = 0$, $\gamma = 2$. (*a*) Newtonian: *PD* (◯), *VD* (+), *Pr* (▽), total (−). (*b*) $W = 1$: *PD* (◯), *VD* (+), *Pr* (▽), *PD* + *VD* (△), total (−), *VD* (Newtonian) (×). (*c*) $W = 12$: *PD* (◯), *VD* (+), *Pr* (▽), *PD* + *VD* (△), total (−), *VD* (Newtonian) (×), *Pr* (Newtonian) (□), total (Newtonian) (- - -).

the effect of the polymer additives on the instability mechanisms. An extensive parameter study was conducted by varying the polymer relaxation time, the polymer concentration and the maximum extensibility of the polymer chains L for the FENE-P closure.

The main finding has been that the effect of the polymer can be characterized by the ratio between the relaxation time and the time scale over which the instability evolves; this applies to the exponential growth of two-dimensional Tollmien–Schlichting-like waves and to the non-modal amplification of streamwise elongated streaks and oblique waves in the subcritical regime. For both types of disturbances, we recorded destabilization for small values of this ratio, i.e. relatively short relaxation times, and stabilization for large values. The maximum destabilization was observed for values of the ratio between the polymer relaxation time and the instability time scale of order unity.

Modal analysis

The non-monotonic behaviour of the critical Reynolds number as a function of Weissenberg number W, already documented for Oldroyd-B fluids by Sadanandan & Sureshkumar (2002), Stone *et al.* (2004) and Roy *et al.* (2006), is recovered here for the FENE-P model as well. This is explained by considering the work of the

Reynolds stress against the base flow shear. At $W\omega_r \lesssim 1$ the polymer molecules can be considered as inelastic and the total dissipation in the flow is not changed. However, the polymer elasticity alters the phase shift between streamwise and wall-normal velocity fluctuations, leading to an increased production of perturbation kinetic energy and to a more unstable flow. Our results indicate that the destabilization observed at short polymer relaxation times is proportional to the polymer viscosity. At larger $W\omega_r$, the polymers have time to be stretched, the elastic effects are more relevant and the flow becomes more stable, as shown by the reduction of the kinetic energy production against the mean shear. We show how the increased/decreased production of perturbation kinetic energy is related to the phase lag between the wall-normal and streamwise velocity fluctuations, as observed previously for inelastic non-Newtonian fluids (Nouar, Bottaro & Brancher 2007).

It is instructive to relate the effect of viscosity at the critical layer to previous results pertaining to inelastic fluids with shear-dependent viscosity. Govindarajan, Lõvov & Procaccia (2001) study the stability of channel flow with space-dependent viscosity at the critical layer and find a large stabilization due to a reduced energy intake from the mean flow to the fluctuations in the case of reduced viscosity, and the opposite for larger viscosity in regions of higher shear. Ranganathan & Govindarajan (2005) and Nouar *et al.* (2007) used the Carreau model and showed that shear-thinning fluids are more stable. These authors explain their results by the base flow modifications induced by a varying viscosity and by the effect on the Reynolds stresses near the critical layer. Unlike these previous studies, we consider polymer additives on a fixed base flow, namely the parabolic profile, and therefore examine only the effect of elasticity. In all cases the production increases at the critical layer: this is associated with a local increase of the viscosity as in shear-thickening fluids, and indeed the destabilization is shown to scale with the polymer viscosity. For long relaxation times, however, we find that the elastic effects manifest themselves with negative production above the critical layer and in the centre of the channel. Eventually, this effect outweighs the increased production at the critical layer and the flow becomes more stable.

Non-modal analysis

A similar trend is observed for the non-modal growth of perturbations in the subcritical regime. Previous investigations considered the flow response to stochastic excitations, focusing on the Oldroyd-B model and on streamwise independent disturbances (see Hoda *et al.* 2008, 2009; Jovanović & Kumar 2010, 2011). Our analyses examined both streamwise independent and oblique disturbances. The transient growth of streamwise independent modes, or streaks, is still the dominant instability. The associated energy growth is found to increase monotonically when W increases. For finite α, the maximum amplification G_{max} slightly increases at $W \leqslant 1$, and decreases with increasing W. In the latter case, the data for G_{max} are also found to collapse when they are presented versus W/T_{max}, where T_{max} is the time at which the maximum growth is observed. Again we observe destabilization if the disturbance amplifies on a time scale longer than the polymer relaxation time and a stabilization when the disturbance growth is characterized by a time scale shorter than the polymer relaxation.

The energy analysis reveals that the increase of the transient growth of streamwise invariant disturbances (vanishing α) is due to an increased production against the mean shear at early times. Similarly, the initial decrease of production of the disturbance energy is responsible for the reduced growth observed for larger values of α (see figure 9). This suggests that a similar argument can explain both modal and non-modal

amplification. The importance of oblique modes in the laminar–turbulence transition should not be underestimated: these are the dominant modes excited by a localized disturbance. In addition, as shown in Klinkenberg *et al.* (2013) for particle-laden flows, damping of oblique modes can have a two-fold effect on transition: (i) it can delay transition and require a larger initial disturbance amplitude to cause breakdown as oblique modes are weaker and, as a result, the interactions transferring energy to the streamwise independent streaky modes are also attenuated; (ii) it can delay the transition time, since less energy is available to disrupt the streamwise independent streaks resulting from the optimal non-modal amplification in subcritical conditions.

The effects summarized above are enhanced for lower values of the viscosity ratio β, larger polymer viscosity, and the variations of the modal and non-modal disturbance amplification are found to vary linearly with the polymer viscosity. Increasing elastic effects by increasing the maximum extensibility of the polymer molecules, L, destabilizes exponential instabilities, while it has a marginal effect on the non-modal amplification.

The present results apply to the initial disturbance evolution in transitional wall-bounded shear flows of viscoelastic fluids. To speculate on the consequences for the full transition process, it is worthwhile drawing an analogy to the case of particle-laden flows (Klinkenberg *et al.* 2011, 2013). At relatively high volume fractions, these flows present both drag reduction in the turbulent regime and attenuation of oblique modes in the linear regime (while nothing dramatic happens to the non-modal growth of streaks). Moreover, the turbulent regime of both polymer and particle solutions is characterized by intervals of 'hibernating' (low-activity) turbulence characterized by weak streamwise vortices and nearly non-existent streamwise variations (Xi & Graham 2010; Zhao, Andersson & Gillissen 2010). In the case of particle suspensions these two aspects appear to be related and associated with a certain transition delay (increase of the threshold energy for transition). We therefore suggest extending the present work in the nonlinear regime by investigating the full transition process and the link between the linear response and the transition to turbulence, as our results seem to indicate an analogy with the case of rigid particles.

Appendix. Matrices of the linear stability problem

In this appendix we provide the full equations describing the linear stability of the Oldroyd-B and FENE-P fluid in the wall-normal velocity and wall-normal vorticity formulation

$$\frac{\partial}{\partial t}\boldsymbol{A}\tilde{\phi} = \boldsymbol{B}\tilde{\phi}, \tag{A 1}$$

where the vector $\tilde{\phi} = (\tilde{v}, \tilde{\eta}, \tilde{c}_{11}, \tilde{c}_{22}, \tilde{c}_{33}, \tilde{c}_{12}, \tilde{c}_{13}, \tilde{c}_{23})^{\mathrm{T}}$. The matrix $\boldsymbol{A}$ is the same for both viscoelastic models, $\begin{pmatrix} \boldsymbol{A}_{11} & 0 \\ 0 & \boldsymbol{I}_6 \end{pmatrix}$. $\boldsymbol{A}_{11}$, of dimensions 2×2, pertains to the fluid velocity and vorticity, and is identical to that derived for the O–S and Sq equations:

$$\begin{pmatrix} \Delta & 0 \\ 0 & \boldsymbol{I} \end{pmatrix}, \tag{A 2}$$

where $\Delta = \mathrm{D}^2 - k^2$, with D the derivative with respect to the wall-normal direction and the wavenumber $k^2 = \alpha^2 + \gamma^2$. The unity matrix $\boldsymbol{I}_6$ here has dimension 6×6 and is related to the six components of the conformation tensor.

The matrix $\boldsymbol{B}$ can be written as $\begin{pmatrix} \boldsymbol{B}_{11} & \boldsymbol{B}_{12} \\ \boldsymbol{B}_{21} & \boldsymbol{B}_{22} \end{pmatrix}$. $\boldsymbol{B}_{11}$ is the same as in the single phase O–S and Sq equations, and is given by

$$\begin{pmatrix} \dfrac{\beta}{Re}\Delta^2 - \mathrm{i}\alpha U\Delta + \mathrm{i}\alpha U'' & 0 \\ -\mathrm{i}\beta U' & \dfrac{\beta}{Re}\Delta - \mathrm{i}\alpha U \end{pmatrix}. \tag{A 3}$$

$\boldsymbol{B}_{21}$ expresses the effect of the disturbance velocity field on the polymer stretching:

$$\boldsymbol{B}_{21} = \frac{1}{k^2}\begin{pmatrix} 2(-\alpha^2 C_{11}\mathrm{D} + \mathrm{i}\alpha C_{12}\mathrm{D}^2) - k^2\mathrm{D}C_{11} & 2(\alpha\gamma C_{11} - \mathrm{i}\gamma C_{12}\mathrm{D}) \\ 2k^2(\mathrm{i}\alpha C_{12} + C_{22}\mathrm{D}) - k^2\mathrm{D}C_{22} & 0 \\ -2\gamma^2 C_{33}\mathrm{D} - k^2\mathrm{D}C_{33} & -2\alpha\gamma C_{33} \\ k^2(\mathrm{i}\alpha C_{11} + C_{12}\mathrm{D}) - k^2\mathrm{D}C_{12} & \alpha\gamma C_{12} - \mathrm{i}\gamma C_{22}\mathrm{D} \\ +\mathrm{i}\alpha C_{22}\mathrm{D}^2 - \alpha^2 C_{12}\mathrm{D} & \\ -\alpha\gamma C_{11}\mathrm{D} + \mathrm{i}\gamma C_{12}\mathrm{D}^2 - \alpha\gamma C_{33}\mathrm{D} & -\alpha^2 C_{11} + \mathrm{i}\alpha C_{12}\mathrm{D} + \gamma^2 C_{33} \\ \mathrm{i}\gamma C_{22}\mathrm{D}^2 - \alpha\gamma C_{12}\mathrm{D} + \mathrm{i}k^2\gamma C_{33} & -\alpha^2 C_{12} + \mathrm{i}\alpha C_{22}\mathrm{D} \end{pmatrix}, \tag{A 4}$$

where $\mathrm{D}C_{ij} = \mathrm{d}C_{ij}/\mathrm{d}y$ and we have exploited the symmetry of the conformation tensor.

The remaining blocks depend on the particular model used for the viscoelastic properties of the fluid. $\boldsymbol{B}_{12}$ represents the polymeric stresses in the momentum equation, and for the Oldroyd-B model is given by

$$\boldsymbol{B}_{12} = \frac{1-\beta}{WRe}\begin{pmatrix} \alpha^2\mathrm{D} & -k^2\mathrm{D} & \gamma^2\mathrm{D} & -\mathrm{i}\alpha(\mathrm{D}^2 + k^2) & 2\alpha\gamma\mathrm{D} & -\mathrm{i}\gamma(\mathrm{D}^2 + k^2) \\ -\alpha\gamma & 0 & \alpha\gamma & \mathrm{i}\gamma\mathrm{D} & \alpha^2 - \gamma^2 & -\mathrm{i}\alpha\mathrm{D} \end{pmatrix}. \tag{A 5}$$

For the same model, the polymer relaxation, transport and stretching by the base flow is expressed by

$$\boldsymbol{B}_{22} = \begin{pmatrix} K_{ob} & 0 & 0 & 2U' & 0 & 0 \\ 0 & K_{ob} & 0 & 0 & 0 & 0 \\ 0 & 0 & K_{ob} & 0 & 0 & 0 \\ 0 & U' & 0 & K_{ob} & 0 & 0 \\ 0 & 0 & 0 & 0 & K_{ob} & U' \\ 0 & 0 & 0 & 0 & 0 & K_{ob} \end{pmatrix}. \tag{A 6}$$

U' indicates the first derivative of the base flow U along the wall-normal direction y and $K_{ob} = -\mathrm{i}\alpha U - 1/W$.

For the FENE-P model,

$$\boldsymbol{B}_{12} = \begin{pmatrix} vc_{11} & vc_{22} & vc_{33} & vc_{12} & vc_{13} & vc_{23} \\ \eta c_{11} & \eta c_{22} & \eta c_{33} & \eta c_{12} & \eta c_{13} & \eta c_{23} \end{pmatrix}, \tag{A 7}$$

and we adopt the following notation:

$$C'_{11} = \frac{\mathrm{d}C_{11}}{\mathrm{d}y}, \quad C'_{22} = \frac{\mathrm{d}C_{22}}{\mathrm{d}y}, \quad C'_{33} = \frac{\mathrm{d}C_{33}}{\mathrm{d}y}, \tag{A 8a}$$

$$C''_{11} = \frac{d^2 C_{11}}{\mathrm{d}y^2}, \quad C''_{22} = \frac{d^2 C_{22}}{\mathrm{d}y^2}, \quad C''_{33} = \frac{d^2 C_{33}}{\mathrm{d}y^2}, \tag{A 8b}$$

$$f'_1 = \left.\frac{\partial f}{\partial C_{11}}\right|_{\boldsymbol{B}} = f'_2 = \left.\frac{\partial f}{\partial C_{22}}\right|_{\boldsymbol{B}} = f'_3 = \left.\frac{\partial f}{\partial C_{33}}\right|_{\boldsymbol{B}} = \frac{L^2}{(L^2 - C_{kk})^2}, \tag{A 9a}$$

$$f'_y = f'_1 C'_{11} + f'_2 C'_{22} + f'_3 C'_{33}, \tag{A 9b}$$

$$f''_{1y} = \frac{\partial^2 f}{\partial C_{11}\partial y} = f''_{2y} = \frac{\partial^2 f}{\partial C_{22}\partial y} = f''_{3y} = \frac{\partial^2 f}{\partial C_{33}\partial y} = \frac{2L^2}{(L^2 - C_{kk})^3}(C'_{11} + C'_{22} + C'_{33}), \tag{A 9c}$$

$$\begin{aligned} f'''_{1yy} &= \frac{\partial^3 f}{\partial C_{11}\partial y^2} = f'''_{2yy} = \frac{\partial^3 f}{\partial C_{22}\partial y^2} = f'''_{3yy} = \frac{\partial^3 f}{\partial C_{33}\partial y^2}, \\ &= \frac{6L^2}{(L^2 - C_{kk})^4}(C'_{11} + C'_{22} + C'_{33})^2 + \frac{2L^2}{(L^2 - C_{kk})^3}(C''_{11} + C''_{22} + C''_{33}). \end{aligned} \tag{A 9d}$$

The different terms in $\boldsymbol{B}_{12}$ can then be written as follows, where for greater clarity we use the symbol $*$ to denote multiplication:

$$\begin{aligned} vc_{11} = \frac{1-\beta}{ReW}[&-k^2(f'_1 * C_{21} * \mathrm{i}\alpha + f''_{1y} * C_{22} + f'_1 * C_{22} * \mathrm{D} + f'_1 * C_{23} * \mathrm{i}\gamma + f'_1 * C'_{22}) \\ &- \mathrm{i}\alpha(f''_{1y} * C_{11} * \mathrm{i}\alpha + f'_1 * C_{11} * \mathrm{i}\alpha * \mathrm{D} + f'_1 * C'_{11} * \mathrm{i}\alpha + f'''_{1yy} * C_{12} \\ &+ f''_{1y} * C_{12} * \mathrm{D} + f''_{1y} * C'_{12} + f''_{1y} * C_{12} * \mathrm{D} + f'_1 * C_{12} * \mathrm{D}^2 + f'_1 * C'_{12} * \mathrm{D} \\ &+ f''_{1y} * C_{13} * \mathrm{i}\gamma + f'_1 * C_{13} * \mathrm{i}\gamma * \mathrm{D} + f'_1 * C'_{13} * \mathrm{i}\gamma + f''_{1y} * C'_{12} + f'_1 * C'_{12} * \mathrm{D} \\ &+ f'_1 * C''_{12} + f'_y * \mathrm{i}\alpha + f * \mathrm{i}\alpha * \mathrm{D}) - \mathrm{i}\gamma(f''_{1y} * C_{31} * \mathrm{i}\alpha + f'_1 * C_{31} * \mathrm{i}\alpha * \mathrm{D} \\ &+ f'_1 * C'_{31} * \mathrm{i}\alpha + f'''_{1yy} * C_{32} + f''_{1y} * C_{32} * \mathrm{D} + f''_{1y} * C'_{32} + f''_{1y} * C_{32} * \mathrm{D} \\ &+ f'_1 * C_{32} * \mathrm{D}^2 + f'_1 * C'_{32} * \mathrm{D} + f''_{1y} * C_{33} * \mathrm{i}\gamma + f'_1 * C_{33} * \mathrm{i}\gamma * \mathrm{D} \\ &+ f'_1 * C'_{33} * \mathrm{i}\gamma + f''_{1y} * C'_{32} + f'_1 * C'_{32} * \mathrm{D} + f'_1 * C''_{32})], \end{aligned} \tag{A 10}$$

$$\begin{aligned} vc_{22} = \frac{1-\beta}{ReW}[&-k^2(f'_2 * C_{21} * \mathrm{i}\alpha + f''_{2y} * C_{22} + f'_2 * C_{22} * \mathrm{D} + f'_2 * C_{23} * \mathrm{i}\gamma + f'_2 * C'_{22} \\ &+ f'_y + f * \mathrm{D}) - \mathrm{i}\alpha(f''_{2y} * C_{11} * \mathrm{i}\alpha + f'_2 * C_{11} * \mathrm{i}\alpha * \mathrm{D} + f'_2 * C'_{11} * \mathrm{i}\alpha \\ &+ f'''_{2yy} * C_{12} + f''_{2y} * C_{12} * \mathrm{D} + f''_{2y} * C'_{12} + f''_{2y} * C_{12} * \mathrm{D} + f'_2 * C_{12} * \mathrm{D}^2 \\ &+ f'_2 * C'_{12} * \mathrm{D} + f''_{2y} * C_{13} * \mathrm{i}\gamma + f'_2 * C_{13} * \mathrm{i}\gamma * \mathrm{D} + f'_2 * C'_{13} * \mathrm{i}\gamma \\ &+ f''_{2y} * C'_{12} + f'_2 * C'_{12} * \mathrm{D} + f'_2 * C''_{12}) - \mathrm{i}\gamma(f''_{2y} * C_{31} * \mathrm{i}\alpha + f'_2 * C_{31} * \mathrm{i}\alpha * \mathrm{D} \\ &+ f'_2 * C'_{31} * \mathrm{i}\alpha + f'''_{2yy} * C_{32} + f''_{2y} * C_{32} * \mathrm{D} + f''_{2y} * C'_{32} + f''_{2y} * C_{32} * \mathrm{D} \\ &+ f'_2 * C_{32} * \mathrm{D}^2 + f'_2 * C'_{32} * \mathrm{D} + f''_{2y} * C_{33} * \mathrm{i}\gamma + f'_2 * C_{33} * \mathrm{i}\gamma * \mathrm{D} \\ &+ f'_2 * C'_{33} * \mathrm{i}\gamma + f''_{2y} * C'_{32} + f'_2 * C'_{32} * \mathrm{D} + f'_2 * C''_{32})], \end{aligned} \tag{A 11}$$

$$\begin{aligned} vc_{33} = \frac{1-\beta}{ReW}[&-k^2(f'_3 * C_{21} * \mathrm{i}\alpha + f''_{3y} * C_{22} + f'_3 * C_{22} * \mathrm{D} + f'_3 * C_{23} * \mathrm{i}\gamma + f'_3 * C'_{22}) \\ &- \mathrm{i}\alpha(f''_{3y} * C_{11} * \mathrm{i}\alpha + f'_3 * C_{11} * \mathrm{i}\alpha * \mathrm{D} + f'_3 * C'_{11} * \mathrm{i}\alpha + f'''_{3yy} * C_{12} + f''_{3y} * C_{12} * \mathrm{D} \\ &+ f''_{3y} * C'_{12} + f''_{3y} * C_{12} * \mathrm{D} + f'_3 * C_{12} * \mathrm{D}^2 + f'_3 * C'_{12} * \mathrm{D} + f''_{3y} * C_{13} * \mathrm{i}\gamma \\ &+ f'_3 * C_{13} * \mathrm{i}\gamma * \mathrm{D} + f'_3 * C'_{13} * \mathrm{i}\gamma + f''_{3y} * C'_{12} + f'_3 * C'_{12} * \mathrm{D} + f'_3 * C''_{12}) \\ &- \mathrm{i}\gamma(f''_{3y} * C_{31} * \mathrm{i}\alpha + f'_3 * C_{31} * \mathrm{i}\alpha * \mathrm{D} + f'_3 * C'_{31} * \mathrm{i}\alpha + f'''_{3yy} * C_{32} + f''_{3y} * C_{32} * \mathrm{D} \\ &+ f''_{3y} * C'_{32} + f''_{3y} * C_{32} * \mathrm{D} + f'_3 * C_{32} * \mathrm{D}^2 + f'_3 * C'_{32} * \mathrm{D} + f''_{3y} * C_{33} * \mathrm{i}\gamma \\ &+ f'_3 * C_{33} * \mathrm{i}\gamma * \mathrm{D} + f'_3 * C'_{33} * \mathrm{i}\gamma + f''_{3y} * C'_{32} + f'_3 * C'_{32} * \mathrm{D} \\ &+ f'_3 * C''_{32} + f'_y * \mathrm{i}\gamma + f * \mathrm{i}\gamma * \mathrm{D})], \end{aligned} \tag{A 12}$$

$$vc_{12} = \frac{1-\beta}{ReW}[-k^2 * f * \mathrm{i}\alpha - \mathrm{i}\alpha(f''_{1y} * C'_{11} + f'_1 * C''_{11} + f'_1 * C'_{11} * \mathrm{D} + f''_{2y} * C'_{22} + f'_2 * C''_{22} + f'_2 * C'_{22} * \mathrm{D} + f''_{3y} * C'_{33} + f'_3 * C''_{33} + f'_3 * C'_{33} * \mathrm{D} + f'_y * \mathrm{D} + f * \mathrm{D}^2)], \tag{A 13}$$

$$vc_{13} = \frac{1-\beta}{ReW}[-\mathrm{i}\alpha(f'_y * \mathrm{i}\gamma + f * \mathrm{i}\gamma * \mathrm{D}) - \mathrm{i}\gamma(f'_y * \mathrm{i}\alpha + f * \mathrm{i}\alpha * \mathrm{D})], \tag{A 14}$$

$$vc_{23} = \frac{1-\beta}{ReW}[-k^2 * f * \mathrm{i}\gamma - \mathrm{i}\gamma(f''_{1y} * C'_{11} + f'_1 * C''_{11} + f'_1 * C'_{11} * \mathrm{D} + f''_{2y} * C'_{22} + f'_2 * C''_{22} + f'_2 * C'_{22} * \mathrm{D} + f''_{3y} * C'_{33} + f'_3 * C''_{33} + f'_3 * C'_{33} * \mathrm{D} + f'_y * \mathrm{D} + f * \mathrm{D}^2)], \tag{A 15}$$

$$\eta c_{11} = \frac{1-\beta}{ReW}[\mathrm{i}\gamma(f'_1 * C_{11} * \mathrm{i}\alpha + f''_{1y} * C_{12} + f'_1 * C_{12} * \mathrm{D} + f'_1 * C_{13} * \mathrm{i}\gamma + f'_1 * C'_{12} + f * \mathrm{i}\alpha) - \mathrm{i}\alpha(f'_1 * C_{31} * \mathrm{i}\alpha + f''_{1y} * C_{32} + f'_1 * C_{32} * \mathrm{D} + f'_1 * C_{33} * \mathrm{i}\gamma + f'_1 * C'_{32})], \tag{A 16}$$

$$\eta c_{22} = \frac{1-\beta}{ReW}[\mathrm{i}\gamma(f'_2 * C_{11} * \mathrm{i}\alpha + f''_{2y} * C_{12} + f'_2 * C_{12} * \mathrm{D} + f'_2 * C_{13} * \mathrm{i}\gamma + f'_2 * C'_{12}) - \mathrm{i}\alpha(f'_2 * C_{31} * \mathrm{i}\alpha + f''_{2y} * C_{32} + f'_2 * C_{32} * \mathrm{D} + f'_2 * C_{33} * \mathrm{i}\gamma + f'_2 * C'_{32})], \tag{A 17}$$

$$\eta c_{33} = \frac{1-\beta}{ReW}[\mathrm{i}\gamma(f'_3 * C_{11} * \mathrm{i}\alpha + f''_{3y} * C_{12} + f'_3 * C_{12} * \mathrm{D} + f'_3 * C_{13} * \mathrm{i}\gamma + f'_3 * C'_{12}) - \mathrm{i}\alpha(f'_3 * C_{31} * \mathrm{i}\alpha + f''_{3y} * C_{32} + f'_3 * C_{32} * \mathrm{D} + f'_3 * C_{33} * \mathrm{i}\gamma + f'_3 * C'_{32} + f * \mathrm{i}\gamma)], \tag{A 18}$$

$$\eta c_{12} = \frac{1-\beta}{ReW}[\mathrm{i}\gamma(f'_y + f * \mathrm{D})], \tag{A 19}$$

$$\eta c_{13} = \frac{1-\beta}{ReW}[\mathrm{i}\gamma * f * \mathrm{i}\gamma - \mathrm{i}\alpha * f * \mathrm{i}\alpha], \tag{A 20}$$

$$\eta c_{23} = \frac{1-\beta}{ReW}[-\mathrm{i}\alpha(f'_y + f * \mathrm{D})]. \tag{A 21}$$

Finally,

$$\boldsymbol{B}_{22} = \begin{pmatrix} K_{fp} + J_1 * C_{11} & J_2 * C_{11} & J_3 * C_{11} & 2U' & 0 & 0 \\ J_1 * C_{22} & K_{fp} + J_2 * C_{22} & J_3 * C_{22} & 0 & 0 & 0 \\ J_1 * C_{33} & J_2 * C_{33} & K_{fp} + J_3 * C_{33} & 0 & 0 & 0 \\ J_1 * C_{12} & U' + J_2 * C_{12} & J_3 * C_{12} & K_{fp} & 0 & 0 \\ J_1 * C_{13} & J_2 * C_{13} & J_3 * C_{13} & 0 & K_{fp} & U' \\ J_1 * C_{23} & J_2 * C_{23} & J_3 * C_{23} & 0 & 0 & K_{fp} \end{pmatrix}, \tag{A 22}$$

where $J_i = -f'_i/W$ and $K_{fp} = -\mathrm{i}\alpha U - f/W$.

REFERENCES

ARORA, K. & KHOMAMI, B. 2005 The influence of finite extensibility on the eigenspectrum of dilute polymeric solutions. *J. Non-Newtonian Fluid Mech.* **129**, 56–60.

ARRATIA, P. E., THOMAS, C. C., DIORIO, J. & GOLLUB, J. P. 2006 Elastic instabilities of polymer solutions in cross-channel flow. *Phys. Rev. Lett.* **96**, 144502.

ATALIK, K. & KEUNINGS, R. 2002 Non-linear temporal stability analysis of viscoelastic plane channel flows using a fully-spectral method. *J. Non-Newtonian Fluid Mech.* **102**, 209–319.

BERLIN, S., LUNDBLADH, A. & HENNINGSON, D. S. 1994 Spatial simulations of oblique transition. *Phys. Fluids* **6**, 1949–1951.

BERTI, S., BISTAGNINO, A., BOFFETTA, G., CELANI, A. & MUSACCHIO, S. 2008 Two-dimensional elastic turbulence. *Phys. Rev.* E **77**, 055306.

BIRD, R., CURTISS, C., ARMSTRONG, R. & HASSAGER, O. 1987 *Dynamics of Polymer Liquids. Vol. 2. Kinetic Theory*. Wiley.

BISTAGNINO, A., BOFFETTA, G., CELANI, A., MAZZINO, A., PULIAFITO, A. & VERGASSOLA, M. 2007 Nonlinear dynamics of the viscoelastic Kolmogorov flows. *J. Fluid Mech.* **590**, 61–80.

BLONCE, L. 1997 Linear stability of Giesekus fluids in Poiseuille flow. *Mech. Res. Commun.* **24**, 223–228.

BURGHELEA, T., SEGRE, E. & STEINBERG, V. 2006 Role of elastic stress in statistical and scaling properties of elastic turbulence. *Phys. Rev. Lett.* **96**, 214502.

BUTLER, K. M. & FARRELL, B. F. 1992 Three-dimensional optimal perturbations in viscous shear flow. *Phys. Fluids* A **4** (8), 1637–1650.

CANUTO, C. G., HUSSAINI, M. Y., QUARTERONI, A. & ZANG, T. A. 2007 *Spectral Methods: Evolution of Complex Geometries and Applications to Fluid Mechanics*. Springer.

CRUZ, D., PINHO, F. & OLIVEIRA, P. 2005 Analytical solutions for fully developed laminar flow of some viscoelastic liquids with a Newtonian solvent contribution. *J. Non-Newtonian Fluid Mech.* **132**, 28–35.

DE ANGELIS, E., CASCIOLA, C. M. & PIVA, R. 2002 DNS of wall turbulence: dilute polymers and self-sustaining mechanisms. *Comput. Fluids* **31**, 495–507.

DOERING, C. R., ECKHARDT, B. & SCHUMACHER, J. 2006 Failure of energy stability in Oldroyd-B fluids at arbitrarily low Reynolds numbers. *J. Non-Newtonian Fluid Mech.* **135**, 92–96.

DUBIEF, Y., WHITE, C. M., TERRAPON, V. E., SHAQFEH, E. S. G., MOIN, P. & LELE, S. K. 2004 On the coherent drag-reducing and turbulence-enhancing behaviour of polymers in wall flows. *J. Fluid Mech.* **514**, 271–280.

DUGUET, Y., BRANDT, L. & LARSSON, B. R. J. 2010 Towards minimal perturbations in transitional plane Couette flow. *Phys. Rev.* E **82**, 026316.

FARRELL, B. F. 1988 Optimal excitation of perturbations in viscous shear flow. *Phys. Fluids* **31** (8), 2093–2102.

FARRELL, B. F. & IOANNOU, P. J. 1993 Optimal excitation of three-dimensional constant shear flow. *Physics* **5** (6), 1390–1400.

GOVINDARAJAN, R., LÕVOV, V. S. & PROCACCIA, I. 2001 Retardation of the onset of turbulence by minor viscosity contrasts. *Phys. Rev. Lett.* **87** (17).

GROISMAN, A. & STEINBERG, V. 2001 Elastic turbulence in a polymer solution flow. *Nature* **405** (6782), 53–55.

GROISMAN, A. & STEINBERG, V. 2004 Elastic turbulence in curvilinear flows of polymer. *New J. Phys.* **6**, 29.

HO, T. C. & DENN, M. M. 1977 Stability of plane Poiseuille flow of a highly elastic liquid. *J. Non-Newtonian Fluid Mech.* **3**, 179–195.

HODA, N., JOVANOVIĆ, M. R. & KUMAR, S. 2008 Energy amplification in channel flows of viscoelastic fluids. *J. Fluid Mech.* **601**, 407–424.

HODA, N., JOVANOVIC, M. R. & KUMAR, S. 2009 Frequency responses of streamwise-constant perturbations in channel flows of Oldroyd-B fluids. *J. Fluid Mech.* **625**, 411–434.

HUERRE, P. & ROSSI, M. 1998 Hydrodynamic instabilities in open flows. In *Hydrodynamic and Nonlinear Instabilities* (ed. C. Godrèche & P. Manneville), pp. 81–294. Cambridge University Press.

JOO, Y. L. & SHAQFEH, S. G. 1992 The effects of inertia on the viscoelastic Dean and Taylor–Couette flow instabilities with application to coating flows. *Phys. Fluids* **4**, 2415–2431.

JOVANOVIĆ, M. R. & KUMAR, S. 2010 Transient growth without inertia. *Phys. Fluids* **22** (2)023101.

JOVANOVIĆ, M. R. & KUMAR, S. 2011 Nonmodal amplification of stochastic disturbances in strongly elastic channel flows. *J. Non-Newtonian Fluid Mech.* **166** (14/15), 755–778.

KLINKENBERG, J., DE LANGE, H. C. & BRANDT, L. 2011 Modal and non-modal stability of particle-laden channel flow. *Phys. Fluids* **23** (6)064110.

KLINKENBERG, J., SARDINA, G., LANGE, H. C. D. & BRANDT, L. 2013 Numerical study of laminar–turbulent transition in particle-laden channel flow. *Phys. Rev.* E **86**, 043011.

LARSON, R. G. 1992 Instabilities in viscoelastic flows. *Rheol. Acta* **31** (3), 213–263.

LARSON, R. G. 2000 Turbulence without inertia. *Nature* **405**, 27–28.

LARSON, R. G., SHAQFEH, E. S. G. & MULLER, S. J. 1990 A purely viscoelastic instability in Taylor–Couette flow. *J. Fluid Mech.* **218**, 573–600.

LIEU, B. K., JOVANOVIC, M. R. & KUMAR, S. 2013 Worst-case amplification of disturbances in inertialess Couette flow of viscoelastic fluids. *J. Fluid Mech.* **723**, 232–263.

MEULENBROEK, B., STORM, C., MOROZOV, A. N. & SAARLOOS, W. 2004 Weakly nonlinear subcritical instability of visco-elastic Poiseuille flow. *J. Non-Newtonian Fluid Mech.* **116**, 235–268.

MOROZOV, A. N. & SAARLOOS, W. 2005 Subcritical finite-amplitude solutions for plane Couette flow of viscoelastic fluids. *Phys. Rev. Lett.* **95**, 024501.

NOUAR, C., BOTTARO, A. & BRANCHER, J. P. 2007 Delaying transition to turbulence in channel flow: revisiting the stability of shear-thinning fluids. *J. Fluid Mech.* **592**, 177–194.

PORTEOUS, K. C. & DENN, M. M. 1972 Linear stability of plane Poiseuille flow of viscoelastic liquids. *Trans. Soc. Rheol.* **16** (2), 295–308.

RANGANATHAN, B. T. & GOVINDARAJAN, R. 2005 Stabilization and destabilization of channel flow by location of viscosity-stratified fluid layer. *Phys. Fluids* **13** (1).

REDDY, S. C., SCHMID, P. J. & HENNINGSON, D. S. 1993 Pseudospectra of the Orr–Sommerfeld operator. *SIAM J. Appl. Maths* **53** (1), 15–47.

RENARDY, M. & RENARDY, Y. 1986 Linear stability of plane Couette flow of an upper convected Maxwell fluid. *J. Non-Newtonian Fluid Mech.* **22**, 23–33.

ROY, A., MOROZOV, A., SAARLOOS, W. V. & LARSON, R. G. 2006 Mechanism of polymer drag reduction using a low-dimensional model. *Phys. Rev. Lett.* **97**, 234501.

SADANANDAN, B. & SURESHKUMAR, R. 2002 Viscoelastic effects on the stability of wall-bounded shear flows. *Phys. Fluids* **14** (1), 41–48.

SCHMID, P. J. & HENNINGSON, D. S. 2001 *Stability and Transition in Shear Flows*. Springer.

SHAQFEH, E. S. G. 1996 Purely elastic instabilities in viscometric flows. *Annu. Rev. Fluid Mech.* **28**, 129–185.

STONE, P. A., ROY, A., LARSON, R. G., WALEFFE, F. & GRAHAM, M. D. 2004 Polymer drag reduction in exact coherent structures of plane shear flow. *J. Phys. Fluids* **16** (9), 3470–3482.

SURESHKUMAR, R. & BERIS, A. N. 1995 Linear stability analysis of viscoelastic Poiseuille flow using an Arnoldi-based orthogonalization algorithm. *J. Non-Newtonian Fluid Mech.* **56** (2), 151–182.

SURESHKUMAR, R., SMITH, M. D., ARMSTRONG, R. C. & BROWN, R. A. 1999 Linear stability and dynamics of viscoelastic flows using time-dependent numerical simulations. *J. Non-Newtonian Fluid Mech.* **82**, 57–104.

TOMS, B. A. 1949 Some observations of the flow of linear polymer solution through straight tubes at large Reynolds numbers. In *Proceedings of the First International Congress on Rheology (North-Holland, Amsterdam, 1949),* vol. 2, pp. 135–141.

TREFETHEN, N., TREFETHEN, A. E., REDDY, S. C. & DRISCOLL, T. A. 1993 Hydrodynamic stability without eigenvalues. *Science* **261**, 578–584.

WEIDEMAN, J. A. & REDDY, S. C. 2000 A MATLAB differentiation matrix suite. *ACM Trans. Math. Softw.* **26**, 465–519.

WHITE, C. M. & MUNGAL, M. G. 2008 Mechanics and prediction of turbulent drag reduction with polymer additives. *Annu. Rev. Fluid Mech.* **40**, 235–256.

XI, L. & GRAHAM, M. D. 2010 Turbulent drag reduction and multistage transitions in viscoelastic minimal flow units. *J. Fluid Mech.* **647**, 421–452.

ZHAO, L. H., ANDERSSON, H. I. & GILLISSEN, J. J. J. 2010 Turbulence modulation and drag reduction by spherical particles. *Phys. Fluids* **22**, 081702.

ZHU, L., LAUGA, E. & BRANDT, L. 2011 Self-propulsion in viscoelastic fluids: pushers vs. pullers. *Phys. Fluids* **24**, 051902.